Weighted azimuthal asymmetries in a diquark spectator model

Alessandro Bacchetta,[1,2,*] Marco Radici,[2,†] Francesco Conti,[1,2,‡] and Marco Guagnelli[2,§]

[1] *Dipartimento di Fisica Nucleare e Teorica, Università di Pavia, I-27100 Pavia, Italy*
[2] *Istituto Nazionale di Fisica Nucleare, Sezione di Pavia, I-27100 Pavia, Italy*

(Dated: March 5, 2010)

We analytically calculate weighted azimuthal asymmetries in semi-inclusive lepton-nucleon deep-inelastic scattering and Drell–Yan processes, using transverse-momentum-dependent partonic densities obtained in a diquark spectator model. We compare the asymmetries with available preliminary experimental data, in particular for the Collins and the Sivers effect. We make predictions for other cases of interest in running and planned experiments.

PACS numbers: 12.39.-x, 13.60.-r, 13.88.+e

I. INTRODUCTION

Azimuthal asymmetries correspond to cross-section modulations depending on the azimutal angles involved in the process. Most of the time they are also spin asymmetries, in the sense that these azimuthal modulations appear with opposite sign when the spin of one of the participating particles is reversed. They are essential tools to study partonic transverse-momentum distributions (TMDs), defined as probabilities to find inside a hadron a parton with longitudinal momentum fraction x and transverse momentum $\boldsymbol{p}_T$ with respect to the direction of the parent hadron momentum [1]. TMDs can be used to construct a three-dimensional picture of partons inside hadrons in momentum space and may be related to the orbital angular momentum of partons [2–9].

In a recent paper, we published our results for all leading-twist TMDs in the context of a spectator model of the nucleon, using scalar and axial-vector diquarks, and further distinguishing between different isospin projections (ud and uu) [10]. The free parameters were fixed by reproducing the parametrizations of Ref. [11] and [12] for the unpolarized and helicity distributions at the lowest available scale, respectively, the latter being assumed as the model scale. Nonvanishing odd structures with respect to naïve time-reversal transformations (for brevity, T-odd TMDs), were generated by approximating the gauge-link operator with a single gluon-exchange interaction, representing the rescattering of the struck quark with the spectator diquark at leading order in the strong coupling constant α_s. Compared to our original publication, in this work we have modified the value we chose for α_s at the model scale: instead of an *ad-hoc* nonperturbative value, we have computed it using renormalization-group equations at leading-order (LO). This change has the effect of resizing all T-odd functions by a global constant.

A first test would be to calculate the $\boldsymbol{p}_T$ dependence of unpolarized cross sections, either in semi-inclusive deep-inelastic scattering (SIDIS) or in Drell–Yan hadronic collisions. However, asymmetries are usually preferable, because, being defined as ratios of cross-section combinations, are less sensitive to systematic errors and to theoretical uncertainties as well.

Two types of azimutal asymmetries are commonly considered: weighted and unweighted. From the experimental point of view, unweighted asymmetries are easier and safer to measure. There is by now a good amount of data, mainly on single-spin asymmetries (SSA) in SIDIS [13, 14]. Experimental data for weighted SSA are scarce, with low statistics, and still preliminary [15]. However, from the theoretical side unweighted asymmetries are more complex because transverse momenta are intertwined in a convolution that can be broken only by assuming a specific $\boldsymbol{p}_T$ distribution, typically Gaussian. Weighted asymmetries are preferable: they can be written in a model-independent way in terms of "collinear" objects — parton distribution functions (PDFs) or $\boldsymbol{p}_T$ moments of TMDs, and analogously for fragmentation functions [16]. Most of the time, this simplifies the theoretical treatment, allows a simpler study of factorization and scale evolution, and allows more freedom beyond the choice of a Gaussian ansatz for TMDs.

In fact, our model TMDs display a $\boldsymbol{p}_T$ distribution which is not Gaussian (while also displaying a strong flavor dependence and strong $x-\boldsymbol{p}_T$ correlations) [10]: as such, it does not allow to analytically work out unweighted SSA as

*Electronic address: alessandro.bacchetta@unipv.it
†Electronic address: marco.radici@pv.infn.it
‡Electronic address: francesco.conti@pv.infn.it
§Electronic address: marco.guagnelli@pv.infn.it

simple products of terms, and requires a numerical approach [17] (see also the approximations discussed in Ref. [18]). On the contrary, weighted asymmetries in our model can be always calculated analytically.

For what concerns the scale evolution, equations are known only for the first $\boldsymbol{p}_T$ moment of the Sivers function function [19–21], and have a non-diagonal form that makes their treament more difficult than for the standard collinear PDFs. In order to include some evolution effects while avoiding these complications, we compute the moment of the Sivers function at different scales using only the diagonal part of its evolution equations, and we extend this treatment also to the other TMD moments.

For all the above reasons, we choose to calculate weighted azimuthal (spin) asymmetries and to compare with the few available data: the double-spin asymmetry A_{LL} in SIDIS with longitudinally polarized protons [22], the Collins and the Sivers effect in SIDIS [15], all measured by the HERMES collaboration. There are also A_{LL} data collected by the HERMES and COMPASS collaborations with a deuteron target (see for example Ref. [23]), but in this paper we will consider only measurements directly on a proton target. We will show predictions, instead, for other cases of interest in view of running or future experiments. For example, at JLab the E06-010 experiment [24] is measuring the Collins and the Sivers effects using the 6 GeV energy beam hitting on a transversely polarized ^{3}He (effective neutron) target, in order to extract the neutron transversity distribution. As for Drell–Yan, the fully polarized process with antiprotons is planned to be measured at FAIR (GSI), in order to perform a self-consistent extraction of the transversity distribution [25–29]; while the COMPASS collaboration is planning to measure a SSA using a high energetic pion beam on a transversely polarized proton target at CERN [30–33], where the T-odd Sivers function could be extracted and its predicted non-universal behaviour directly tested [34].

The paper is organized as follows. In Sec. II, the kinematics and the formulae for the weighted azimuthal (spin) asymmetries in SIDIS and Drell–Yan are briefly illustrated. In Sec. III, the formalism and the analytic results for T-even and T-odd TMDs in the spectator diquark model of Ref. [10] are recalled. In Sec. IV, the updated model T-odd TMDs are compared with the available parametrizations and the weighted SSA are compared with the few SIDIS experimental data, making predictions for asymmetries in the Drell–Yan process and for other cases of interest.

II. WEIGHTED AZIMUTHAL (SPIN) ASYMMETRIES

In the following we will make use of light-cone coordinates. We introduce the light-like vectors $n_\pm$ satisfying $n_\pm^2 = 0$, $n_+ \cdot n_- = 1$, and we describe a generic 4-vector $a = [a^-, a^+, \boldsymbol{a}_T]$, where $a^\pm = a \cdot n_\mp$. We will also make use of the transverse tensor $\epsilon_T^{ij} = \epsilon^{\mu\nu ij} n_{+\mu} n_{-\nu}$, whose only nonvanishing components are $\epsilon_T^{12} = -\epsilon_T^{21} = 1$.

We consider the SIDIS process of a lepton on a (polarized) nucleon, as well as hadronic collisions leading to Drell–Yan lepton pairs.

A. SIDIS

In a SIDIS process a (polarized) lepton with momentum l is scattered to a final momentum l' by a nucleon target with mass M, momentum P, and spin S, leaving also a final hadron semi-inclusively produced with mass M_h and momentum P_h. The 4-momentum transferred is denoted by $q = l - l'$, with $Q^2 = -q^2$. We introduce the invariants

$$x = \frac{Q^2}{2P \cdot q} \approx \frac{p^+}{P^+} , \qquad y = \frac{P \cdot q}{P \cdot l} , \qquad z = \frac{P \cdot P_h}{P \cdot q} \approx \frac{P_h^-}{k^-} , \tag{1}$$

where $k = p + q$, and p is the momentum of the parton before the scattering. We choose a set of frames where P has no transverse components, i.e.,

$$P = \left[\frac{M^2}{2P^+}, P^+, \boldsymbol{0} \right] . \tag{2}$$

Hence, the target polarization 4-vector and the parton momentum can be parametrized as

$$\begin{aligned} S &= \left[-\frac{\lambda_h M}{2P^+}, \frac{\lambda_h P^+}{M}, \boldsymbol{S}_\perp \right] , \\ p &= \left[\frac{p^2 + \boldsymbol{p}_T^2}{2xP^+}, xP^+, \boldsymbol{p}_T \right] , \end{aligned} \tag{3}$$

with λ_h the hadron helicity. Analogously, λ_e represents the incoming lepton helicity.

In single-photon-exchange approximation, the cross section can be parametrized in terms of 18 structure functions [35]. Here we are concerned with the regime $Q^2 \gg \boldsymbol{P}_{h\perp}^2, M^2$. An analysis based on TMD factorization reveals that only the following 8 structure functions are present at leading order in a M^2/Q^2 expansion (twist expansion) [1]:

$$\begin{aligned}\frac{d\sigma}{dxdydzd\phi_S d\phi_h d\boldsymbol{P}_{h\perp}^2} = \frac{\alpha^2}{s}\left(1+\frac{\gamma^2}{2x}\right)\Big\{&A(x,y)\,F_{UU} + B(x,y)\,\cos(2\phi_h)\,F_{UU}^{\cos 2\phi_h} \\ &+ \lambda_h\, B(x,y)\,\sin(2\phi_h)\,F_{UL}^{\sin 2\phi_h} + \lambda_h\,\lambda_e\,C(x,y)\,F_{LL} \\ &+ |\boldsymbol{S}_\perp|\Big[A(x,y)\,\sin(\phi_h-\phi_S)\,F_{UT}^{\sin(\phi_h-\phi_S)} + B(x,y)\,\sin(\phi_h+\phi_S)\,F_{UT}^{\sin(\phi_h+\phi_S)} \\ &+ B(x,y)\,\sin(3\phi_h-\phi_S)\,F_{UT}^{\sin(3\phi_h-\phi_S)}\Big] + |\boldsymbol{S}_\perp|\,\lambda_e\,C(x,y)\,\cos(\phi_h-\phi_S)\,F_{LT}^{\cos(\phi_h-\phi_S)}\Big\}\,,\end{aligned} \tag{4}$$

where α is the fine structure constant, $s = Q^2/xy$ is the center-of-mass energy squared, $\gamma = 2Mx/Q$, ϕ_h, ϕ_S, are the azimuthal orientations of $\boldsymbol{P}_h$ and $\boldsymbol{S}$ with respect to the scattering plane, respectively (see Fig. 1; for their formal definition, see Eqs.(2.3)-(2.6) in Ref. [35]), and

$$A(x,y) = \frac{1}{x^2y^2\,(1+\gamma^2)}\,\left(1-y+\tfrac{1}{2}y^2+\tfrac{1}{4}y^2\gamma^2\right)\,, \tag{5}$$

$$B(x,y) = \frac{1}{x^2y^2\,(1+\gamma^2)}\,\left(1-y-\tfrac{1}{4}y^2\gamma^2\right)\,, \tag{6}$$

$$C(x,y) = \frac{1}{x^2y^2\,\sqrt{1+\gamma^2}}\,y(1-\tfrac{1}{2}y)\,. \tag{7}$$

Note that the above expressions include mass corrections, related to γ, and the factor $1/(x^2y^2)$, which must not be dropped when integrating separately numerator and denominator of the asymmetries (see Sec. IV).

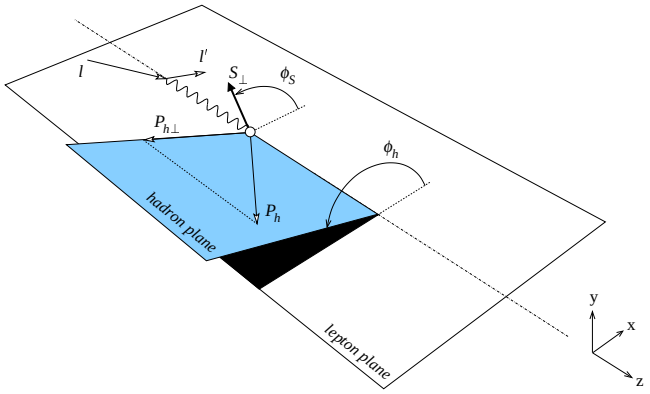

FIG. 1: The kinematics of the semi-inclusive deep-inelastic scattering.

In Eq. (4), each contribution F_{XY}^W depends on $x, z, \boldsymbol{P}_{h\perp}^2$, and on Q^2; it refers to a lepton with polarization state X (that can be unpolarized, U, or longitudinally polarized, L, with helicity λ_e), and to a target with polarization state Y (that can be unpolarized, U, longitudinally polarized, L, with helicity λ_h, and transversely polarized, T, with polarization $|\boldsymbol{S}_\perp|$). The superscript W refers to the azimuthal distribution of detected hadrons. At leading order in

[1] Since we are keeping only the leading-twist contribution, we have shortened the original notation $F_{UU,T}$, $F_{UT,T}^{\sin(\phi_h-\phi_S)}$, of Ref. [35] to F_{UU}, $F_{UT}^{\sin(\phi_h-\phi_S)}$, since we are not sensitive to longitudinally polarized virtual photons.

the strong coupling (LO) and leading twist, the structure functions read [35]

$$
\begin{aligned}
F_{UU} &= \mathcal{C}\Big[f_1 D_1\Big] \,, \\
F_{UU}^{\cos 2\phi} &= \mathcal{C}\Big[-\frac{2(\hat{\boldsymbol{h}}\cdot\boldsymbol{k}_T)\,(\hat{\boldsymbol{h}}\cdot\boldsymbol{p}_T)-\boldsymbol{k}_T\cdot\boldsymbol{p}_T}{MM_h}\,h_1^\perp\,H_1^\perp\Big] \,, \\
F_{UL}^{\sin 2\phi} &= \mathcal{C}\Big[-\frac{2(\hat{\boldsymbol{h}}\cdot\boldsymbol{k}_T)\,(\hat{\boldsymbol{h}}\cdot\boldsymbol{p}_T)-\boldsymbol{k}_T\cdot\boldsymbol{p}_T}{MM_h}\,h_{1L}^\perp\,H_1^\perp\Big] \,, \\
F_{LL} &= \mathcal{C}\Big[g_{1L}\,D_1\Big] \,, \\
F_{UT}^{\sin(\phi_h-\phi_S)} &= \mathcal{C}\Big[-\frac{\hat{\boldsymbol{h}}\cdot\boldsymbol{p}_T}{M}\,f_{1T}^\perp\,D_1\Big] \,, \\
F_{UT}^{\sin(\phi_h+\phi_S)} &= \mathcal{C}\Big[-\frac{\hat{\boldsymbol{h}}\cdot\boldsymbol{k}_T}{M_h}\,h_1\,H_1^\perp\Big] \,, \\
F_{UT}^{\sin(3\phi_h-\phi_S)} &= \mathcal{C}\Big[\frac{2(\hat{\boldsymbol{h}}\cdot\boldsymbol{p}_T)\,(\boldsymbol{k}_T\cdot\boldsymbol{p}_T)+\boldsymbol{p}_T^2\,(\hat{\boldsymbol{h}}\cdot\boldsymbol{k}_T)-4(\hat{\boldsymbol{h}}\cdot\boldsymbol{p}_T)^2\,(\hat{\boldsymbol{h}}\cdot\boldsymbol{k}_T)}{2M^2M_h}\,h_{1T}^\perp\,H_1^\perp\Big] \,, \\
F_{LT}^{\cos(\phi_h-\phi_S)} &= \mathcal{C}\Big[\frac{\hat{\boldsymbol{h}}\cdot\boldsymbol{p}_T}{M}\,g_{1T}\,D_1\Big] \,,
\end{aligned}
\tag{8}
$$

where $\hat{\boldsymbol{h}} = \boldsymbol{P}_{h\perp}/|\boldsymbol{P}_{h\perp}|$, and the convolution is defined by

$$
\mathcal{C}\Big[w\,f\,D\Big] = x\sum_a e_a^2 \int d\boldsymbol{p}_T d\boldsymbol{k}_T\,\delta^{(2)}(\boldsymbol{p}_T-\boldsymbol{k}_T-\boldsymbol{P}_{h\perp}/z)\,w(\boldsymbol{p}_T,\boldsymbol{k}_T)\,f^a(x,\boldsymbol{p}_T^2)\,D^a(z,\boldsymbol{k}_T^2) \,, \tag{9}
$$

with the sum running over all parton and antiparton flavors a.

The different structure functions can be extracted thanks to their specific dependence on the azimuthal angles. Upon integration in $d\boldsymbol{P}_{h\perp}^2$, only the convolutions in F_{UU} and F_{LL} can be solved analytically, because of the simple weight $w = 1$. In this case, the well known double-spin asymmetry can be formed,

$$
A_{LL} = \frac{C(x,y)}{A(x,y)}\,\frac{\int d\boldsymbol{P}_{h\perp}^2\,F_{LL}}{\int d\boldsymbol{P}_{h\perp}^2\,F_{UU}} = \frac{C(x,y)}{A(x,y)}\,\frac{\sum_a e_a^2\,x g_1^a(x)\,D_1^a(z)}{\sum_a e_a^2\,x f_1^a(x)\,D_1^a(z)} \equiv \frac{C(x,y)}{A(x,y)}\,A_1 \,, \tag{10}
$$

giving access to the helicity distribution $g_1^a(x) = \int d\boldsymbol{p}_T\,g_{1L}^a(x,\boldsymbol{p}_T^2)$. This asymmetry is analyzed in Sec. IV B.

In the other cases, an analytical solution can be achieved only with a suitable model dependence upon $\boldsymbol{p}_T$ and $\boldsymbol{k}_T$ of the distribution and fragmentation functions, respectively [16]. The most widely used Ansatz is a Gaussian distribution in $\boldsymbol{p}_T$ and $\boldsymbol{k}_T$ (usually also assumed to be flavor independent and independent of x and z). It allows an analytic calculation of all convolutions in Eq. (9). However, theoretical calculations indicate that perturbative corrections generate non-Gaussian tails of the TMDs when $\boldsymbol{P}_{h\perp}^2 \gg M^2$ [36] and available experimental data poorly constrain the $\boldsymbol{p}_T$ dependence of partonic densities in general, leaving room for Ansätze different from the Gaussian one. Actually, our model displays a $\boldsymbol{p}_T$ distribution which is not factorized, has a strong flavor dependence, and above all is not Gaussian [10]. As such, it does not allow to analytically calculate all the convolutions in Eq. (9). In this paper we will consider only properly $\boldsymbol{P}_{h\perp}-$weighted asymmetries, which break the convolutions in a model-independent way and result in factorized expressions such as the one in Eq. (10). We leave the computation of unweighted asymmetries to a future work, where we will consider a direct (numerical) calculation of all the convolutions needed in Eq. (8) [17].

Weighted asymmetries are defined as [37]

$$
A_{XY}^W(x,y,z) \propto \frac{\langle W\rangle_{XY}}{\langle 1\rangle_{UU}} \equiv \frac{\int d\phi_S d\phi_h d\boldsymbol{P}_{h\perp}^2\,W\,d\sigma_{XY}}{\int d\phi_S d\phi_h d\boldsymbol{P}_{h\perp}^2\,d\sigma_{UU}} \,, \tag{11}
$$

where $d\sigma_{XY}$ refers to the contribution in Eq. (4) for the lepton probe with polarization X and nucleon target with polarization Y. Typically, the weight W can be function of ϕ_S, ϕ_h, and of suitable powers of $Q_T = |\boldsymbol{P}_{h\perp}|/z$.

For SIDIS, the following weighted azimuthal asymmetries are relevant and theoretically clean [37]:

$$A_{UT}^{Q_T\,\sin(\phi_h+\phi_S)} = 2\,\frac{\left\langle \frac{Q_T}{M_h}\,\sin(\phi_h+\phi_S)\right\rangle_{UT}}{\langle 1\rangle_{UU}} = 2\,\frac{B(x,y)}{A(x,y)}\,\frac{\sum_a e_a^2\,x h_1^a(x)\,H_1^{\perp(1)a}(z)}{\sum_a e_a^2\,x f_1^a(x)\,D_1^a(z)}\,, \tag{12}$$

$$A_{UT}^{Q_T\,\sin(\phi_h-\phi_S)} = 2\,\frac{\left\langle \frac{Q_T}{M}\,\sin(\phi_h-\phi_S)\right\rangle_{UT}}{\langle 1\rangle_{UU}} = -2\,\frac{A(x,y)}{A(x,y)}\,\frac{\sum_a e_a^2\,x f_{1T}^{\perp(1)a}(x)\,D_1^a(z)}{\sum_a e_a^2\,x f_1^a(x)\,D_1^a(z)}\,, \tag{13}$$

$$A_{LT}^{Q_T\,\cos(\phi_h-\phi_S)} = 2\,\frac{\left\langle \frac{Q_T}{M}\,\cos(\phi_h-\phi_S)\right\rangle_{UT}}{\langle 1\rangle_{UU}} = 2\,\frac{C(x,y)}{A(x,y)}\,\frac{\sum_a e_a^2\,x g_{1T}^{(1)a}(x)\,D_1^a(z)}{\sum_a e_a^2\,x f_1^a(x)\,D_1^a(z)}\,, \tag{14}$$

where

$$f^{(n)}(x) = \int d\boldsymbol{p}_T \left(\frac{\boldsymbol{p}_T^2}{2M^2}\right)^n f(x,\boldsymbol{p}_T^2) \tag{15}$$

is the n-th $\boldsymbol{p}_T$-moment of a parton distribution f (and analogously for a fragmentation function).

In every parton density above (or $\boldsymbol{p}_T$ moment of it), the dependence on the hard scale Q^2 is understood. Evolution effects with running Q^2 are well known for f_1, g_1, h_1, and D_1. From the discussion in Sec. 7.3 of Ref. [36] and the explicit study of Ref. [20], it should be evident why we can hope to study the weighted asymmetries (12 - 14) in a way similar to the double-spin asymmetry of Eq. (10), including the scale dependence of the involved functions. Explicit calculations are available only for the evolution equations of the Sivers function $f_{1T}^{\perp(1)}$ [19–21]. They are nondiagonal and thus considerably more complex than those of twist-2 collinear PDFs. However, their diagonal part is identical to the evolution equations for f_1 and should be dominant at high x [20]. Calculations of the real perturbative contributions in g_{1T} [38] suggest that the evolution equations for this function will have a diagonal part identical to that of g_1. In summary, we approximately implement the effect of scale evolution in the weighted asymmetries (12 - 14) by evolving $f_{1T}^{\perp(1)}(x)$ and $g_{1T}^{(1)}(x)$ using the same LO evolution of $f_1(x)$ and $g_1(x)$ (see, e.g., Ref. [39]). For $H_1^{\perp(1)}(z)$, we used the same LO evolution as the transversity fragmentation function $H_1(z)$ (see, e.g., Ref. [40]). The asymmetries (12 - 14) are considered in Sec. IV B.

In our analysis, we will not take into consideration the following asymmetries

$$A_{UU}^{Q_T^2\,\cos 2\phi_h} = 2\,\frac{\left\langle \frac{Q_T^2}{4MM_h}\,\cos 2\phi_h\right\rangle_{UU}}{\langle 1\rangle_{UU}} \overset{\text{TMD}}{=} 2\,\frac{B(x,y)}{A(x,y)}\,\frac{\sum_a e_a^2\,x h_1^{\perp(1)a}(x)\,H_1^{\perp(1)a}(z)}{\sum_a e_a^2\,x f_1^a(x)\,D_1^a(z)}\,, \tag{16}$$

$$A_{UL}^{Q_T^2\,\sin 2\phi_h} = 2\,\frac{\left\langle \frac{Q_T^2}{4MM_h}\,\sin 2\phi_h\right\rangle_{UL}}{\langle 1\rangle_{UU}} \overset{\text{TMD}}{=} 2\,\frac{B(x,y)}{A(x,y)}\,\frac{\sum_a e_a^2\,x h_{1L}^{\perp(1)a}(x)\,H_1^{\perp(1)a}(z)}{\sum_a e_a^2\,x f_1^a(x)\,D_1^a(z)}\,, \tag{17}$$

$$A_{UT}^{Q_T^3\,\sin(3\phi_h-\phi_S)} = 2\,\frac{\left\langle \frac{Q_T^3}{6M^2M_h}\,\sin(3\phi_h-\phi_S)\right\rangle_{UT}}{\langle 1\rangle_{UU}} \overset{\text{TMD}}{=} 2\,\frac{B(x,y)}{A(x,y)}\,\frac{\sum_a e_a^2\,x h_{1T}^{\perp(2)a}(x)\,H_1^{\perp(1)a}(z)}{\sum_a e_a^2\,x f_1^a(x)\,D_1^a(z)}\,, \tag{18}$$

$$\tag{19}$$

because the higher powers of Q_T in the weight emphasize the high-$\boldsymbol{p}_T$ components of the asymmetry, that are dominated by perturbative QCD corrections [36] and do not give enough information about TMDs. In the above equations, we nevertheless gave the explicit expressions for these weighted asymmetries in the TMD framework, since it might still be possible to isolate their TMD component by means of differences, or ratios between different measurements, that cancel the perturbative contributions. We will not discuss these possibilities in the present work.

B. Drell–Yan

In a Drell–Yan process, a pair with individual momenta k_1 and k_2, formed by a lepton and its antilepton partner, is produced from the collision of two hadrons with momentum P_i, mass M_i, and spin S_i, with $i = 1, 2$. The cm square energy available is $s = (P_1 + P_2)^2$; the momentum transfer is now time-like and gives the invariant mass of the pair, i.e.

$$q^2 \equiv M^2 = (k_1 + k_2)^2 = (p_1 + p_2)^2\,, \tag{20}$$

where p_i are the momenta of the annihilating partons, with $i = 1, 2$. If P_1^+ and P_2^- are the dominant light-cone components of hadron momenta in the regime where the factorization theorem holds [41], we can define the following invariants:

$$x_1 = \frac{q^2}{2P_1 \cdot q} \approx \frac{p_1^+}{P_1^+} , \qquad x_2 = \frac{q^2}{2P_2 \cdot q} \approx \frac{p_2^-}{P_2^-} ,$$
$$y = \frac{k_1 \cdot P_1}{q \cdot P_1} \approx \frac{k_1^-}{q^-} , \quad \tau = \frac{M^2}{s} , \quad x_F = x_1 - x_2 . \tag{21}$$

We choose x_1 as the momentum fraction of the parton in the beam; namely,

$$x_1 = \tfrac{1}{2}\left(x_F + \sqrt{x_F^2 + 4\tau}\right) = \sqrt{\tau}\, e^y ,$$
$$x_2 = \tfrac{1}{2}\left(-x_F + \sqrt{x_F^2 + 4\tau}\right) = \sqrt{\tau}\, e^{-y} . \tag{22}$$

In the following, we will plot SSA as functions of x_F and/or y at a given τ: this choice will probe very different regions in x_1 and x_2, where the model parton distributions involved behave very differently. And this feature will show up clearly in the asymmetry.

Because of momentum conservation, the 4-momentum transfer can be parametrized as

$$q = \left[x_2 P_2^-, x_1 P_1^+, \boldsymbol{p}_{1T} + \boldsymbol{p}_{2T}\right] . \tag{23}$$

If the transverse momentum of the final lepton pair is $\boldsymbol{q}_T = \boldsymbol{p}_{1T} + \boldsymbol{p}_{2T} \neq 0$, the directions of the two annihilating partons are not known. Hence, it is convenient to select the socalled Collins-Soper frame [42] described in Fig. 2. The final lepton pair is detected in the solid angle (θ, ϕ), where, in particular, ϕ (and all other azimuthal angles) is measured in a plane perpendicular to the indicated lepton plane but containing $\hat{\boldsymbol{h}} = \boldsymbol{q}_T/|\boldsymbol{q}_T| \equiv \boldsymbol{q}_T/q_T$.

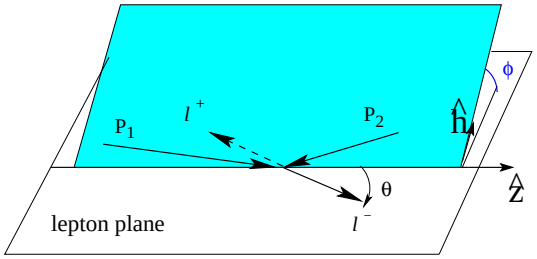

FIG. 2: The Collins-Soper frame.

The fully differential LO cross section can contain many contributions according to the polarization state of the two colliding hadrons [43]. Having in mind the phenomenology that could be explored at GSI-FAIR and CERN, or at J-PARC and RHIC, we limit the physics case to the most relevant combinations. The master channel is the $\bar{p}^\uparrow p^\uparrow \to l^+ l^- X$ reaction [25–27], whose polarized q_T-integrated cross section is simply [44]

$$\frac{d\tilde{\sigma}^{\uparrow\uparrow}}{d\Omega dx_1 dx_2} = \frac{\alpha^2}{3q^2} |\boldsymbol{S}_{1T}|\, |\boldsymbol{S}_{2T}|\, \tfrac{1}{4} \sin^2\theta\, \cos(2\phi - \phi_{S_1} - \phi_{S_2})\, \textstyle\sum_a e_a^2\, h_1^{\overline{a}}(x_1)\, h_1^a(x_2) , \tag{24}$$

where $d\Omega = \sin\theta d\theta d\phi$ and $|\boldsymbol{S}_{iT}|$, ϕ_{S_i} are the transverse polarization and the azimuthal angle of its vector for hadron i. Combining Eq. (24) with the unpolarized part, we can form the well known double-spin asymmetry

$$\begin{aligned}
\tilde{A}_{TT} &= \frac{d\tilde{\sigma}^{\uparrow\uparrow} - d\tilde{\sigma}^{\uparrow\downarrow}}{d\tilde{\sigma}^{\uparrow\uparrow} + d\tilde{\sigma}^{\uparrow\downarrow}} \\
&= |\boldsymbol{S}_{1T}|\, |\boldsymbol{S}_{2T}|\, \frac{\sin^2\theta}{1 + \cos^2\theta}\, \cos(2\phi - \phi_{S_1} - \phi_{S_2})\, \frac{\sum_a e_a^2\, x_1 h_1^{\overline{a}}(x_1)\, x_2 h_1^a(x_2)}{\sum_a e_a^2\, x_1 f_1^{\overline{a}}(x_1)\, x_2 f_1^a(x_2)} \\
&\equiv |\boldsymbol{S}_{1T}|\, |\boldsymbol{S}_{2T}|\, \tilde{a}_{TT}\, \frac{\sum_a e_a^2\, x_1 h_1^{\overline{a}}(x_1)\, x_2 h_1^a(x_2)}{\sum_a e_a^2\, x_1 f_1^{\overline{a}}(x_1)\, x_2 f_1^a(x_2)} ,
\end{aligned} \tag{25}$$

which gives direct access to (the valence part of) the transversity distribution h_1. Monte Carlo simulations about the feasibility of this measurement were presented in Ref. [29]. Predictions based on our diquark spectator model will be shown in Sec. IV C.

When in the collision only one hadron can be transversely polarized, the fully differential leading-twist cross section reads [43, 45]

$$\frac{d\tilde{\sigma}}{d\Omega dx_1 dx_2 d\boldsymbol{q}_T} = \frac{\alpha^2}{3q^2}\Bigg\{\tilde{A}(y)\,\tilde{F}_{UU} + \tilde{B}(y)\,\cos(2\phi)\,\tilde{F}_{UU}^{\cos 2\phi} + |\boldsymbol{S}_{2T}|\left[\tilde{A}(y)\,\sin(\phi-\phi_{S_2})\,\tilde{F}_{UT}^{\sin(\phi-\phi_{S_2})} - \tilde{B}(y)\,\sin(\phi+\phi_{S_2})\,\tilde{F}_{UT}^{\sin(\phi+\phi_{S_2})} - \tilde{B}(y)\,\sin(3\phi-\phi_{S_2})\,\tilde{F}_{UT}^{\sin(3\phi-\phi_{S_2})}\right]\Bigg\}, \tag{26}$$

where

$$\tilde{A}(y) = \left(\tfrac{1}{2} - y + y^2\right) \overset{\text{cm}}{=} \tfrac{1}{4}\left(1+\cos^2\theta\right) \qquad \tilde{B}(y) = y(1-y) \overset{\text{cm}}{=} \tfrac{1}{4}\sin^2\theta\,. \tag{27}$$

The structure functions $\tilde{F}_{XY}^W$ depend on x_1, x_2, q_T. They read [43]

$$\begin{aligned}
\tilde{F}_{UU} &= \tilde{\mathcal{C}}\left[1\, f_1\, f_1\right], \\
\tilde{F}_{UU}^{\cos 2\phi} &= \tilde{\mathcal{C}}\left[2\frac{\hat{\boldsymbol{h}}\cdot\boldsymbol{p}_{1T}\,\hat{\boldsymbol{h}}\cdot\boldsymbol{p}_{2T} - \boldsymbol{p}_{1T}\cdot\boldsymbol{p}_{2T}}{M_1 M_2}\, h_1^\perp\, h_1^\perp\right], \\
\tilde{F}_{UT}^{\sin(\phi-\phi_{S_2})} &= \tilde{\mathcal{C}}\left[\frac{\hat{\boldsymbol{h}}\cdot\boldsymbol{p}_{2T}}{M_2}\, f_1\, f_{1T}^\perp\right], \\
\tilde{F}_{UT}^{\sin(\phi+\phi_{S_2})} &= \tilde{\mathcal{C}}\left[\frac{\hat{\boldsymbol{h}}\cdot\boldsymbol{p}_{1T}}{M_1}\, h_1^\perp\, h_1\right], \\
\tilde{F}_{UT}^{\sin(3\phi-\phi_{S_2})} &= \tilde{\mathcal{C}}\left[\frac{4\hat{\boldsymbol{h}}\cdot\boldsymbol{p}_{1T}\,(\hat{\boldsymbol{h}}\cdot\boldsymbol{p}_{2T})^2 - 2\hat{\boldsymbol{h}}\cdot\boldsymbol{p}_{2T}\,\boldsymbol{p}_{1T}\cdot\boldsymbol{p}_{2T} - \hat{\boldsymbol{h}}\cdot\boldsymbol{p}_{1T}\,\boldsymbol{p}_{2T}^2}{2M_1\,M_2^2}\, h_1^\perp\, h_{1T}^\perp\right].
\end{aligned} \tag{28}$$

The convolution $\tilde{\mathcal{C}}$ is defined as

$$\tilde{\mathcal{C}}\left[w\, f\, g\right] = x_1 x_2 \sum_a e_a^2 \int d\boldsymbol{p}_{1T} d\boldsymbol{p}_{2T}\, \delta^{(2)}(\boldsymbol{p}_{1T} + \boldsymbol{p}_{2T} - \boldsymbol{q}_T)\, w(\boldsymbol{p}_{1T}, \boldsymbol{p}_{2T}) \left[f^{\overline{a}}(x_1, \boldsymbol{p}_{1T}^2)\, g^a(x_2, \boldsymbol{p}_{2T}^2)\right]. \tag{29}$$

As in the SIDIS case, only the convolution in $\tilde{F}_{UU}$ can be solved analytically upon integration in $d\boldsymbol{q}_T^2$, because of the simple weight $w = 1$. Again, instead of introducing a suitable model dependence upon transverse momenta, we follow the strategy of considering properly q_T-weighted asymmetries, now defined as

$$\tilde{A}_{XY}^W(x_1, x_2, y) \propto \frac{\langle W\rangle_{XY}}{\langle 1\rangle_{UU}} \equiv \frac{\int d\phi_{S_2} d\phi d\boldsymbol{q}_T^2\, W\, d\tilde{\sigma}_{XY}}{\int d\phi_{S_2} d\phi d\boldsymbol{q}_T^2\, d\tilde{\sigma}_{UU}}\,, \tag{30}$$

where $d\tilde{\sigma}_{XY}$ refers to the contribution in Eq. (26) for the hadrons 1 and 2 with polarizations X and Y, respectively. Typically, the weight W can be function of ϕ_{S_2}, ϕ, and of suitable powers of q_T.

We consider the following weighted asymmetries:

$$\tilde{A}_{UT}^{q_T\,\sin(\phi-\phi_{S_2})} = 2\,\frac{\left\langle \frac{q_T}{M_2}\,\sin(\phi-\phi_{S_2})\right\rangle_{UT}}{\langle 1\rangle_{UU}} = 2\,\frac{\tilde{A}(y)}{\tilde{A}(y)}\,\frac{\sum_a e_a^2\, x_1 f_1^{\overline{a}}(x_1)\, x_2 f_{1T}^{\perp(1)a}(x_2)}{\sum_a e_a^2\, x_1 f_1^{\overline{a}}(x_1)\, x_2 f_1^a(x_2)}\,, \tag{31}$$

$$\tilde{A}_{UT}^{q_T\,\sin(\phi+\phi_{S_2})} = 2\,\frac{\left\langle \frac{q_T}{M_1}\,\sin(\phi+\phi_{S_2})\right\rangle_{UT}}{\langle 1\rangle_{UU}} = -2\,\frac{\tilde{B}(y)}{\tilde{A}(y)}\,\frac{\sum_a e_a^2\, x_1 h_1^{\perp(1)\overline{a}}(x_1)\, x_2 h_1^a(x_2)}{\sum_a e_a^2\, x_1 f_1^{\overline{a}}(x_1)\, x_2 f_1^a(x_2)}\,, \tag{32}$$

For the same considerations expressed in the case of SIDIS, we refrain ourselves from considering the following

asymmetries

$$\tilde{A}_{UU}^{q_T^2\,\cos 2\phi} = 2\,\frac{\left\langle \frac{q_T^2}{4M_1M_2}\,\cos(2\phi)\right\rangle_{UU}}{\langle 1\rangle_{UU}} \overset{\text{TMD}}{=} 2\,\frac{\sum_a e_a^2\,x_1 h_1^{\perp(1)\overline{a}}(x_1)\,x_2 h_1^{\perp(1)a}(x_2)}{\sum_a e_a^2\,x_1 f_1^{\overline{a}}(x_1)\,x_2 f_1^a(x_2)}\,, \tag{33}$$

$$\tilde{A}_{UT}^{q_T^3\,\sin(3\phi-\phi_{S_2})} = 2\,\frac{\left\langle \frac{q_T^3}{6M_1M_2^2}\,\sin(3\phi-\phi_{S_2})\right\rangle_{UT}}{\langle 1\rangle_{UU}} \overset{\text{TMD}}{=} -2\,\frac{\tilde{B}(y)}{\tilde{A}(y)}\,\frac{\sum_a e_a^2\,x_1 h_1^{\perp(1)\overline{a}}(x_1)\,x_2 h_{1T}^{\perp(2)a}(x_2)}{\sum_a e_a^2\,x_1 f_1^{\overline{a}}(x_1)\,x_2 f_1^a(x_2)}\,, \tag{34}$$

where the right-hand-side represents only the TMD contribution to the asymmetry, which is suppressed with respect to perturbative contributions.

Monte Carlo simulations about the feasibility of measurements of the asymmetries (31) and (32) at GSI-FAIR, COMPASS, and RHIC, were presented in Refs. [31, 32, 46, 47]. Predictions based on our diquark spectator model are displayed in Sec. IV C. Similarly, while in Eqs. (31,32) the dependence on the hard scale Q^2 is understood, evolution effects with running Q^2 are included in the same way as discussed at the end of the previous Sec. II A. The chiral-odd function $h_1^{\perp(1)}$ is assumed to follow the same LO evolution equations as the chiral-odd function h_1.

III. T-EVEN AND T-ODD PARTONIC DENSITIES IN A DIQUARK SPECTATOR MODEL

The TMD showing up in Eqs. (12-14) and (31,32) can be calculated analytically in the spectator diquark model. They can be extracted from the basic quantity named quark-quark correlator [35], i.e.

$$\Phi(x,\boldsymbol{p}_T,S) = \int \frac{d\xi^- d\boldsymbol{\xi}_T}{(2\pi)^3}\,e^{ip\cdot\xi}\,\langle P,S|\bar{\psi}(0)\,\mathcal{U}_{[0,\xi]}\,\psi(\xi)|P,S\rangle\Big|_{\xi^+=0}\,, \tag{35}$$

where

$$U_{[0,\xi]} = \mathcal{P}\,e^{-ig\int_0^\xi dw\cdot A(w)} \tag{36}$$

is the socalled gauge link operator connecting the two different space-time points 0 and ξ by a specific path followed by the gluon field A, which couples to the quark field ψ through the coupling g. The gauge link ensures that the matrix element of Eq. (35) is color-gauge invariant.

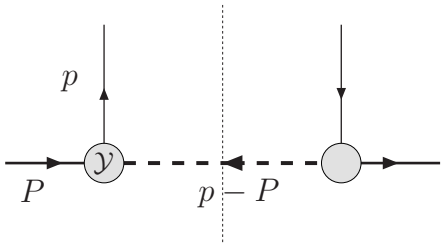

FIG. 3: Tree-level cut diagram for the calculation of T-even leading-twist parton densities. The dashed line indicates both scalar and axial-vector diquarks.

The correlator (35) can be evaluated in the spectator approximation [10, 48]: a completeness relation is inserted and at tree-level the sum over final states is truncated to a single on-shell spectator state with mass M_X (see Fig. 3),

$$\Phi(x,\boldsymbol{p}_T,S) \sim \frac{1}{(2\pi)^3}\,\frac{1}{2(1-x)P^+}\,\overline{\mathcal{M}}^{(0)}(S)\,\mathcal{M}^{(0)}(S)\Big|_{p^2=\tau(x,\boldsymbol{p}_T)}\,, \tag{37}$$

where the on-shell condition $(P-p)^2 = M_X^2$ for the spectator implies for the quark the off-shell condition

$$p^2 \equiv \tau(x,\boldsymbol{p}_T) = -\frac{\boldsymbol{p}_T^2 + L_X^2(m^2)}{1-x} + m^2\,, \qquad L_X^2(m^2) = xM_X^2 + (1-x)m^2 - x(1-x)M^2\,. \tag{38}$$

We assume the spectator to be point-like, with the quantum numbers of a diquark. Hence, the proton can couple to a quark and to a spectator diquark with spin 0 (scalar $X = s$) or spin 1 (axial-vector $X = a$), as well as with

isospin projection 0 (ud-like system) or 1 (uu-like system). Therefore, the tree-level "scattering amplitude" $\mathcal{M}^{(0)}$ is given by (see Fig. 3) [10]

$$\mathcal{M}^{(0)}(S) = \langle P-p|\psi(0)|P,S\rangle = \begin{cases} \dfrac{i}{\not{p}-m}\,\mathcal{Y}_s\,U(P,S) & \text{scalar diquark,} \\ \dfrac{i}{\not{p}-m}\,\varepsilon^*_\mu(P-p,\lambda_a)\,\mathcal{Y}^\mu_a\,U(P,S) & \text{axial-vector diquark,} \end{cases} \tag{39}$$

where the nucleon-quark-diquark vertex can have the form

$$\mathcal{Y}_s = i g_s(p^2)\,\mathbb{1} \quad \text{scalar}\,, \qquad\qquad \mathcal{Y}^\mu_a = i\frac{g_a(p^2)}{\sqrt{2}}\,\gamma^\mu\,\gamma_5 \quad \text{axial-vector}\,, \tag{40}$$

with $g_X(p^2)$ a suitable form factor. The $\varepsilon_\mu(P-p,\lambda_a)$ is the 4-vector polarization of the spin-1 axial-vector diquark with momentum $P-p$ and helicity states λ_a. In Ref. [10], several choices were analyzed for the diquark polarization sum $d^{\mu\nu} = \sum_{\lambda_a} \varepsilon^{*\mu}_{(\lambda_a)}\,\varepsilon^{\nu}_{(\lambda_a)}$ and for the form factor $g_X(p^2)$, with all analytic formulae listed in the appendices. Numerical results were presented only for $d^{\mu\nu}$ propagating transverse diquark polarizations, and for the so-called "dipolar" choice

$$g_X(p^2) = g_X\,\frac{p^2-m^2}{|p^2-\Lambda_X^2|^2} = g_X\,\frac{(p^2-m^2)\,(1-x)^2}{\left(\boldsymbol{p}_T^2 + L_X^2(\Lambda_X^2)\right)^2}\,. \tag{41}$$

Here, we keep the same choices and in the next subsections we list the results for the T-even and T-odd leading-twist TMDs.

A. T-even

The prototype of TMDs is the unpolarized parton distribution, which can be defined in the following way:

$$\begin{aligned} f_1(x,\boldsymbol{p}_T) &= \frac{1}{4}\,\mathrm{Tr}\left[\left(\Phi(x,\boldsymbol{p}_T,S) + \Phi(x,\boldsymbol{p}_T,-S)\right)\,\gamma^+\right] + \text{h.c.} \\ &= \frac{1}{4}\,\frac{1}{(2\pi)^3}\,\frac{1}{2(1-x)P^+}\,\mathrm{Tr}\left[\left(\overline{\mathcal{M}}^{(0)}(S)\,\mathcal{M}^{(0)}(S) + \overline{\mathcal{M}}^{(0)}(-S)\,\mathcal{M}^{(0)}(-S)\right)\,\gamma^+\right] + \text{h.c.}\,, \end{aligned} \tag{42}$$

and can be computed by inserting in $\mathcal{M}^{(0)}$ of Eq. (39) the rules (40) for the nucleon-quark-diquark vertex, the dipolar form factor of Eq. (41), and the diquark polarization sum.

To express in a condensed way all the other TMDs, it is convenient to introduce the two combinations

$$f_1^{+q(s)}(x,\boldsymbol{p}_T^2) \equiv \frac{1}{2}\Big(f_1^{q(s)}(x,\boldsymbol{p}_T^2) + g_{1L}^{q(s)}(x,\boldsymbol{p}_T^2)\Big) = \frac{g_s^2}{(2\pi)^3}\,\frac{(m+xM)^2\,(1-x)^3}{2\,[\boldsymbol{p}_T^2 + L_s^2(\Lambda_s^2)]^4}\,, \tag{43}$$

$$f_1^{-q(s)}(x,\boldsymbol{p}_T^2) \equiv \frac{1}{2}\Big(f_1^{q(s)}(x,\boldsymbol{p}_T^2) - g_{1L}^{q(s)}(x,\boldsymbol{p}_T^2)\Big) = \frac{g_s^2}{(2\pi)^3}\,\frac{\boldsymbol{p}_T^2\,(1-x)^3}{2\,[\boldsymbol{p}_T^2 + L_s^2(\Lambda_s^2)]^4}\,, \tag{44}$$

$$f_1^{+q(a)}(x,\boldsymbol{p}_T^2) \equiv \frac{1}{2}\Big(f_1^{q(a)}(x,\boldsymbol{p}_T^2) + g_{1L}^{q(s)}(x,\boldsymbol{p}_T^2)\Big) = \frac{g_a^2}{(2\pi)^3}\,\frac{\boldsymbol{p}_T^2\,(1+x^2)\,(1-x)}{2\,[\boldsymbol{p}_T^2 + L_a^2(\Lambda_a^2)]^4}\,, \tag{45}$$

$$f_1^{-q(a)}(x,\boldsymbol{p}_T^2) \equiv \frac{1}{2}\Big(f_1^{q(a)}(x,\boldsymbol{p}_T^2) - g_{1L}^{q(a)}(x,\boldsymbol{p}_T^2)\Big) = \frac{g_a^2}{(2\pi)^3}\,\frac{(m+xM)^2\,(1-x)^3}{2\,[\boldsymbol{p}_T^2 + L_a^2(\Lambda_a^2)]^4}\,. \tag{46}$$

Then, the TMDs can be written as (compare with Ref. [10])

$$f_1^{q(s)}(x,\boldsymbol{p}_T^2) = f_1^{+q(s)}(x,\boldsymbol{p}_T^2) + f_1^{-q(s)}(x,\boldsymbol{p}_T^2)\,, \tag{47}$$

$$f_1^{q(a)}(x,\boldsymbol{p}_T^2) = f_1^{+q(a)}(x,\boldsymbol{p}_T^2) + f_1^{-q(a)}(x,\boldsymbol{p}_T^2)\,, \tag{48}$$

$$g_{1L}^{q(s)}(x,\boldsymbol{p}_T^2) = f_1^{+q(s)}(x,\boldsymbol{p}_T^2) - f_1^{-q(s)}(x,\boldsymbol{p}_T^2)\,, \tag{49}$$

$$g_{1L}^{q(a)}(x,\boldsymbol{p}_T^2) = f_1^{+q(a)}(x,\boldsymbol{p}_T^2) - f_1^{-q(a)}(x,\boldsymbol{p}_T^2)\,, \tag{50}$$

$$g_{1T}^{q(s)}(x,\boldsymbol{p}_T^2) = \frac{2M}{m+xM}\, f_1^{+q(s)}(x,\boldsymbol{p}_T^2)\;, \tag{51}$$

$$g_{1T}^{q(a)}(x,\boldsymbol{p}_T^2) = \frac{x}{1-x}\frac{2M}{m+xM}\, f_1^{-q(a)}(x,\boldsymbol{p}_T^2)\;, \tag{52}$$

$$h_{1L}^{\perp\, q(s)}(x,\boldsymbol{p}_T^2) = -g_{1T}^{q(s)}(x,\boldsymbol{p}_T^2)\;, \tag{53}$$

$$h_{1L}^{\perp\, q(a)}(x,\boldsymbol{p}_T^2) = \frac{1}{x}\, g_{1T}^{q(a)}(x,\boldsymbol{p}_T^2)\;, \tag{54}$$

$$h_{1T}^{q(s)}(x,\boldsymbol{p}_T^2) = f_1^{q(s)}(x,\boldsymbol{p}_T^2)\;, \tag{55}$$

$$h_{1T}^{q(a)}(x,\boldsymbol{p}_T^2) = -\frac{2x}{1+x^2}\, f_1^{+q(a)}(x,\boldsymbol{p}_T^2)\;, \tag{56}$$

$$h_{1T}^{\perp\, q(s)}(x,\boldsymbol{p}_T^2) = -\frac{2M^2}{(m+xM)^2}\, f_1^{+q(s)}(x,\boldsymbol{p}_T^2)\;, \tag{57}$$

$$h_{1T}^{\perp\, q(a)}(x,\boldsymbol{p}_T^2) = 0\;, \tag{58}$$

$$h_{1}^{q(s)}(x,\boldsymbol{p}_T^2) = f_1^{+q(s)}(x,\boldsymbol{p}_T^2)\;, \tag{59}$$

$$h_{1}^{q(a)}(x,\boldsymbol{p}_T^2) = h_{1T}^{q(a)}(x,\boldsymbol{p}_T^2)\;. \tag{60}$$

We stress that the previous relations among TMDs should be considered simply as a convenient way to write the results of our model, and should not be considered as general, as can be also deduced by the fact that they are all different in the scalar and axial-vector diquark case. For instance, the relation involving the pretzelosity $h_{1T}^{\perp}$, recently discussed by several authors [7, 49–51], holds in the scalar diquark case, i.e.

$$g_{1L}^{s}(x,\boldsymbol{p}_T) - h_{1}^{s}(x,\boldsymbol{p}_T) = \frac{\boldsymbol{p}_T^2}{2M^2}\, h_{1T}^{\perp\, s}(x,\boldsymbol{p}_T)\;; \tag{61}$$

but it is not true for the axial-vector diquark, as it can be deduced from Eqs. (50), (60), and (58), by noting that $h_{1T}^{\perp\, a} = 0$ (see also Ref. [10]). Therefore, such a relation cannot be totally general.

The $\boldsymbol{p}_T$-integrated results [10] can be expressed in terms of the $\boldsymbol{p}_T$-integrated combinations (43-46):

$$f_1^{+q(s)}(x) = \frac{g_s^2}{(2\pi)^2}\, \frac{2(m+xM)^2\,(1-x)^3}{24\, L_s^6(\Lambda_s^2)}\;, \tag{62}$$

$$f_1^{-q(s)}(x) = \frac{g_s^2}{(2\pi)^2}\, \frac{(1-x)^3}{24\, L_s^4(\Lambda_s^2)}\;, \tag{63}$$

$$f_1^{+q(a)}(x) = \frac{g_a^2}{(2\pi)^2}\, \frac{(1+x^2)\,(1-x)}{24\, L_a^4(\Lambda_a^2)}\;, \tag{64}$$

$$f_1^{-q(a)}(x) = \frac{g_a^2}{(2\pi)^2}\, \frac{2(m+xM)^2\,(1-x)^3}{24\, L_a^6(\Lambda_a^2)}\;. \tag{65}$$

$$\tag{66}$$

The final result is

$$f_1^{q(s)}(x) = f_1^{+q(s)}(x) + f_1^{-q(s)}(x)\;, \tag{67}$$

$$f_1^{q(a)}(x) = f_1^{+q(a)}(x) + f_1^{-q(a)}(x)\;, \tag{68}$$

$$g_1^{q(s)}(x) = f_1^{+q(s)}(x) - f_1^{-q(s)}(x)\;, \tag{69}$$

$$g_1^{q(a)}(x) = f_1^{+q(a)}(x) - f_1^{-q(a)}(x)\;, \tag{70}$$

$$h_1^{q(s)}(x) = f_1^{+q(s)}(x) \,, \tag{71}$$

$$h_1^{q(a)}(x) = -\frac{2x}{1+x^2}\, f_1^{+q(a)}(x) \,. \tag{72}$$

The weighted SSA of Eqs. (14), (17), (18), and (34), require the knowledge also of the following $\boldsymbol{p}_T$-moments:

$$g_{1T}^{q(s)\,(1)}(x) = \frac{g_s^2}{(2\pi)^2}\, \frac{(m+xM)\,(1-x)^3}{24\,M\,L_s^4(\Lambda_s^2)} \,, \tag{73}$$

$$g_{1T}^{q(a)\,(1)}(x) = \frac{g_a^2}{(2\pi)^2}\, \frac{(m+xM)\,x\,(1-x)^2}{24\,M\,L_a^4(\Lambda_a^2)} \,, \tag{74}$$

$$h_{1L}^{\perp q(s)\,(1)}(x) = -g_{1T}^{q(s)\,(1)}(x) \,, \tag{75}$$

$$h_{1L}^{\perp q(a)\,(1)}(x) = \frac{1}{x}\, g_{1T}^{q(a)\,(1)}(x) \,, \tag{76}$$

$$h_{1T}^{\perp q(s)\,(2)}(x) = -\frac{g_s^2}{(2\pi)^2}\, \frac{(1-x)^3}{24\,M^2\,L_s^2(\Lambda_s^2)} \,, \tag{77}$$

$$h_{1T}^{\perp q(a)\,(2)}(x) = 0 \,. \tag{78}$$

For completeness, we also list the $\boldsymbol{p}_T$-moments of the combinations (43-46), which are useful to calculate the mean squared transverse momentum associated to each of the above TMDs:

$$f_1^{+q(s)\,(1)}(x) = \frac{g_s^2}{(2\pi)^2}\, \frac{(m+xM)^2\,(1-x)^3}{96\,M^2\,L_s^4(\Lambda_s^2)} \,, \tag{79}$$

$$f_1^{+q(a)\,(1)}(x) = \frac{g_a^2}{(2\pi)^2}\, \frac{(m+xM)^2\,(1-x)^3}{96\,M^2\,L_a^4(\Lambda_a^2)} \,, \tag{80}$$

$$f_1^{-q(s)\,(1)}(x) = \frac{g_s^2}{(2\pi)^2}\, \frac{2\,(1-x)^3}{96\,M^2\,L_s^2(\Lambda_s^2)} \,, \tag{81}$$

$$f_1^{-q(a)\,(1)}(x) = \frac{g_a^2}{(2\pi)^2}\, \frac{2\,(1+x^2)\,(1-x)}{96\,M^2\,L_a^2(\Lambda_a^2)} \,. \tag{82}$$

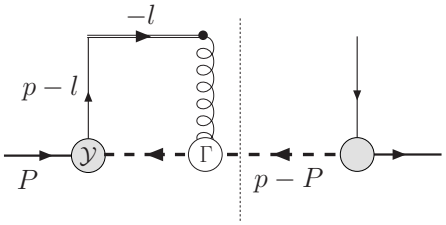

FIG. 4: Interference between the one-gluon exchange diagram in eikonal approximation and the tree level diagram in the spectator model. The Hermitean conjugate diagram is not shown.

B. T-odd

There are only two T-odd structures that can be extracted at leading twist from the quark-quark correlator of Eq. (35), namely

$$\frac{\varepsilon_T^{ij} p_{Ti} S_{Tj}}{M}\, f_{1T}^{\perp}(x, \boldsymbol{p}_T^2) = -\frac{1}{4}\,\mathrm{Tr}\left[\left(\Phi(x,\boldsymbol{p}_T,S) - \Phi(x,\boldsymbol{p}_T,-S)\right)\gamma^+\right] + \mathrm{h.c.} \,, \tag{83}$$

$$\frac{\varepsilon_T^{ij} p_{Tj}}{M}\, h_1^\perp(x, \boldsymbol{p}_T^2) = \frac{1}{4}\,\mathrm{Tr}\left[\left(\Phi(x, \boldsymbol{p}_T, S) + \Phi(x, \boldsymbol{p}_T, -S)\right)\, i\sigma^{i+}\,\gamma_5\right] + \text{h.c.}\,, \tag{84}$$

which are usually referred to as the Sivers [52] and Boer-Mulders [37] functions, respectively.

Using the diagram rules for $\mathcal{M}^{(0)}$ in Fig. 3, from Eq. (37) we find that these expressions vanish at tree level, because there is no interference between two competing channels producing the complex amplitude whose imaginary part gives the T-odd contribution. We can generate such structures by considering the interference between the tree-level scattering amplitude $\mathcal{M}^{(0)}$ and the single-gluon-exchange scattering amplitude $\mathcal{M}^{(1)}$ in eikonal approximation, as shown in Fig. 4 (the Hermitean conjugate partner must also be considered). This corresponds to the one-gluon-exchange approximation of the gauge link operator of Eq. (36) [53].

The Sivers and Boer-Mulders functions can then be rewritten as

$$\frac{\varepsilon_T^{ij} p_{Ti} S_{Tj}}{M}\, f_{1T}^\perp(x, \boldsymbol{p}_T^2) = -\frac{1}{4}\,\frac{1}{(2\pi)^3}\,\frac{1}{2(1-x)P^+}\,\mathrm{Tr}\left[\left(\mathcal{M}^{(1)}(S)\overline{\mathcal{M}}^{(0)}(S) - \mathcal{M}^{(1)}(-S)\overline{\mathcal{M}}^{(0)}(-S)\right)\,\gamma^+\right] + \text{h.c.}\,, \tag{85}$$

$$\frac{\varepsilon_T^{ij} p_{Tj}}{M}\, h_1^\perp(x, \boldsymbol{p}_T^2) = \frac{1}{4}\,\frac{1}{(2\pi)^3}\,\frac{1}{2(1-x)P^+}\,\mathrm{Tr}\left[\left(\mathcal{M}^{(1)}(S)\overline{\mathcal{M}}^{(0)}(S) + \mathcal{M}^{(1)}(-S)\overline{\mathcal{M}}^{(0)}(-S)\right)\, i\sigma^{i+}\,\gamma_5\right] + \text{h.c.}\,. \tag{86}$$

Following the lines of Ref. [10], we come to the final form with scalar and axial vector diquarks:

$$f_{1T}^{\perp\, q(s)}(x, \boldsymbol{p}_T^2) = -g_s^2 C_F \alpha_s\,\frac{M\,\pi}{(2\pi)^4}\,\frac{(1-x)^3\,(m + xM)}{L_s^2(\Lambda_s^2)\,[\boldsymbol{p}_T^2 + L_s^2(\Lambda_s^2)]^3}\,, \tag{87}$$

$$f_{1T}^{\perp\, q(a)}(x, \boldsymbol{p}_T^2) = g_a^2 C_F \alpha_s\,\frac{M\,\pi}{(2\pi)^4}\,\frac{(1-x)^2\,x\,(m + xM)}{L_a^2(\Lambda_a^2)\,[\boldsymbol{p}_T^2 + L_a^2(\Lambda_a^2)]^3}\,, \tag{88}$$

$$h_1^{\perp\, q(s)}(x, \boldsymbol{p}_T^2) = f_{1T}^{\perp\, q(s)}(x, \boldsymbol{p}_T^2)\,, \tag{89}$$

$$h_1^{\perp\, q(a)}(x, \boldsymbol{p}_T^2) = -\frac{1}{x}\, f_{1T}^{\perp\, q(a)}(x, \boldsymbol{p}_T^2)\,, \tag{90}$$

with $C_F = 4/3$.

The high$-\boldsymbol{p}_T$ tail of above expressions could break the positivity bounds [54]. However, the spectator model is supposed to be valid for $\boldsymbol{p}_T^2 \sim M^2$ and for reasonable choices of the parameters no problems with positivity occurr in this region (for more details, see Ref. [10]).

Finally, in the weighted SSA we need the first $\boldsymbol{p}_T$ moments of such functions, which read [10]

$$f_{1T}^{\perp\, q(s)\,(1)}(x) = -\frac{g_s^2}{8}\,\frac{\pi\, C_F \alpha_s}{(2\pi)^3\, M}\,\frac{(m + xM)\,(1-x)^3}{[L_s^2(\Lambda_s^2)]^2}\,, \tag{91}$$

$$f_{1T}^{\perp\, q(a)\,(1)}(x) = \frac{g_a^2}{8}\,\frac{\pi\, C_F \alpha_s}{(2\pi)^3\, M}\,\frac{x\,(m + xM)\,(1-x)^2}{[L_a^2(\Lambda_a^2)]^2}\,, \tag{92}$$

$$h_1^{\perp\, q(s)\,(1)}(x) = f_{1T}^{\perp\, q(s)\,(1)}(x)\,, \tag{93}$$

$$h_1^{\perp\, q(a)\,(1)}(x) = -\frac{1}{x}\, f_{1T}^{\perp\, q(a)\,(1)}(x)\,. \tag{94}$$

IV. RESULTS AND PREDICTIONS

In the following, we present the results for the weighted SSA discussed in Sec. II. We recall that the model parameters were fixed in Ref. [10] by fitting the ZEUS parametrization for f_1^u and f_1^d at the lowest available scale $Q_0^2 = 0.3$ GeV^2 [11], and the GRSV2000 parametrization at LO for g_1^u and g_1^d at $Q_0^2 = 0.26$ GeV^2 [12]. The connection with the model TMDs is realized by

$$\begin{aligned} f_1^u &= c_s^2\, f_1^{u(s)} + c_a^2\, f_1^{u(a)} \\ f_1^d &= c_a'^2\, f_1^{d(a')}\,, \end{aligned} \tag{95}$$

with the coefficients $c_X^{(\prime)}$ given in Tab.I of Ref. [10]. They give the relative probability weight of each quark-diquark configuration in spin and isospin space: scalar-isoscalar diquark s with quark u (c_s), axial vector-isovector diquark

a with isospin projection 0 and quark u (c_a), axial vector-isovector diquark a' with isospin projection 1 and quark d (c'_a).

The model (hadronic) scale is assumed to be $Q_0^2 = 0.3$ GeV^2. At this scale, the contribution of sea over valence quarks is approximately within 10-20% for $x \gtrsim 0.1$; therefore, we have involved only valence contributions in the fitting procedure, keeping in mind that there will be discrepancies at $x < 0.1$. Viceversa, for the D_1 fragmentation function we employ the parametrization of Ref. [55] where both favoured and unfavoured channels are included, the latter being particularly important even at low Q^2. For the Collins function $H_1^\perp$ in Eq. (12), we adopt the analytic expression of Ref. [56], which was obtained in a similar spectator approach as our model TMDs. However, in this case the unfavoured contributions are simply assumed to be equal and opposite to the favoured ones.

Evolution with running Q^2 is implemented by suitably extending the HOPPET code of Ref. [57] to include also chiral-odd partonic densities. The modification is here considered at LO only, and the evolution of all partonic densities will be considered at LO as well in the following, because the factorized expressions of the SSA in Eqs. (12)–(14) and (31),(32) are valid at LO only.

In the following subsection, we reconsider evolution properties of our T-odd TMDs. In the next two subsections, we will present our results for weighted SSA in the SIDIS and in the (polarized) Drell–Yan processes, respectively.

A. Results for model T-odd TMDs

As already anticipated in Sec. II A, evolution equations are not available for all partonic densities in the equations for the considered SSA. At LO, the DGLAP equations for $f_{1T}^{\perp\,(1)}(x)$, $g_{1T}^{(1)}(x)$, $h_1^{\perp\,(1)}(x)$, are assumed to be the same as for $f_1(x)$, $g_1(x)$, $h_1(x)$, respectively.

Moreover, the first $\boldsymbol{p}_T$ moments of these T-odd TMDs depend linearly on α_s [see Eqs. (91)-(94)]. Therefore, a consistent treatment of evolution effects requires to deduce from the LO renormalization group equations the value of α_s at the scale of the hadronic model, Q_0^2, while $\alpha_s(Q_0^2)$ is often considered as a free parameter.

In this sense, in the following we update the results for the model T-odd TMDs with respect to our previous paper [10] by replacing the *ad-hoc* parameter $\alpha_s(Q_0^2) = 0.3$ with the value of $\alpha_s(Q_0^2) = 0.697$ deduced from the LO running of the strong coupling starting from a value of $\alpha(M_Z^2) = 0.125$ (see discussion in Ref. [58]) and using the standard choices of the HOPPET evolution program [57].

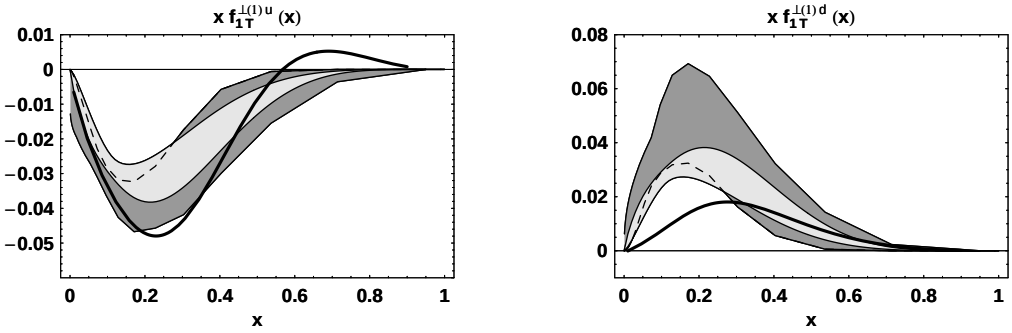

FIG. 5: The first $\boldsymbol{p}_T$ moment $x f_{1T}^{\perp\,(1)}(x)$ of the Sivers function; left (right) panel for up (down) quark. Darker shaded area: statistical uncertainty band of the parametrizations from Ref. [59], lighter shaded area from Ref. [60]. Solid line for the results of the spectator diquark model at the parametrization scale $Q^2 = 2.5$ GeV^2.

In Fig. 5, the first $\boldsymbol{p}_T$ moment $x f_{1T}^{\perp\,(1)}(x)$ of the Sivers function is displayed for the up and down valence quarks in the left and right panels, respectively. The darker shaded area represents the uncertainty due to the statistical error in the parametrization of Ref. [59], while the lighter shaded area corresponds to the same in Ref. [60]. Both parametrizations are deduced by fitting data for the Sivers effect measured by the HERMES [61] and COMPASS [62, 63] collaborations, hence at an average scale $Q^2 = 2.5$ GeV^2. The solid line is given by combining the model results of Eqs. (91) and (92) according to Eq. (95), and by further evolving them at LO from the model scale $Q_0^2 = 0.3$ GeV^2 to the above mentioned parametrization scale.

First of all, we observe the agreement between the signs of the various flavor components, which also agree with the findings from calculations on the lattice [64]. The agreement between model and parametrizations is very good for the up quark, even if the maximum is slightly shifted towards higher x. The size of the function is instead too small for the down quark, and its shape shifted such that the maximum occurs at a higher value of $x \approx 0.3$.

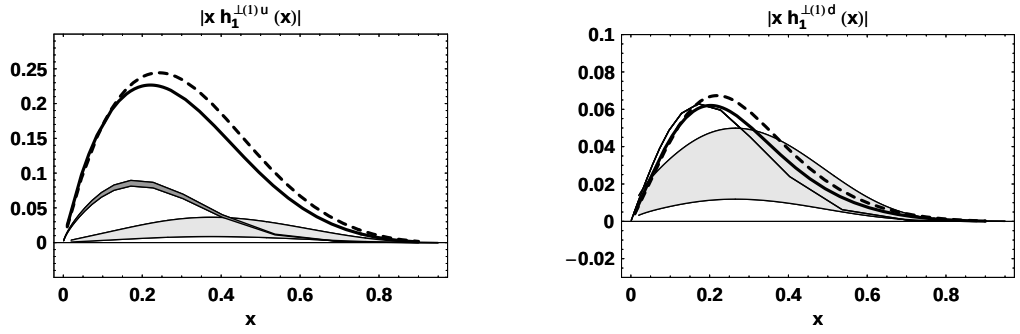

FIG. 6: The modulus of the first $\boldsymbol{p}_T$ moment $|xh_1^{\perp\,(1)}(x)|$ of the Boer–Mulders function; left (right) panel for up (down) quark. Darker shaded area: statistical uncertainty band of the parametrization from Ref. [65], extracted from SIDIS data at $Q^2 = 2.5$ GeV^2. Lighter shaded area: error assigned to parametrization from Ref. [66], extracted from Drell–Yan data at $Q^2 = 1$ GeV^2. Solid and dashed lines for the results of the spectator diquark model evolved at $Q^2 = 2.5$ and 1 GeV^2, respectively. We remark that the results of the spectator diquark model are negative for both up and down quarks (see Ref. [10]); here, we plot their modulus in order to conveniently compare with the published parametrizations.

In Fig. 6, the modulus of the first $\boldsymbol{p}_T$ moment $|xh_1^{\perp\,(1)}(x)|$ of the Boer-Mulders function is displayed for the up and down valence quarks in the left and right panels, respectively. The darker shaded area represents the uncertainty due to the statistical error in the parametrization of Ref. [65], deduced by fitting the $\cos 2\phi$ asymmetry in the unpolarized SIDIS data of Ref. [67–69] at $Q^2 = 2.5$ GeV^2 [see Eq. (16)]. For the down quark, the uncertainty in the fitting parameter is so small that the area reduces to a thin line. The lighter shaded area corresponds to the similar analysis from Ref. [66] but for the unpolarized Drell–Yan data of Ref. [70] at $Q^2 = 1$ GeV^2 [see Eq. (33)]. The solid line is given by combining now the model results of Eqs. (93) and (94) according to Eq. (95), and by further evolving them at LO from the model scale $Q_0^2 = 0.3$ GeV^2 to $Q^2 = 2.5$ GeV^2. The dashed line displays what we obtain when we perform the LO evolution up to $Q^2 = 1$ GeV^2. Hence, the solid line must be compared with the darker shaded area, while the dashed line with the lighter shaded area.

We remark that the $\cos 2\phi$ asymmetry in Drell–Yan involves two Boer–Mulders functions and the fitting procedure cannot fix the sign of the function depending on the flavor involved. The $\cos 2\phi$ asymmetry in SIDIS involves $h_1^\perp$ in combination with the unknown Collins function, whose sign in turn depends on the sign of the transversity h_1. The extraction of Ref. [65] assumes the favoured Collins function to be positive and obtains negative Boer–Mulders functions for both u and d quarks, in agreement with our model [10], with lattice calculations [64], and also with other models [71, 72]. The size of $|xh_1^{\perp\,(1)u}(x)|$ is too high in Fig. 6, while the result for the down quark seems in better agreement with the SIDIS parametrization than with the Drell–Yan one. However, the comparison should be considered with some care because our model results contain only the pure contribution from valence quarks and the data are contaminated by perturbative QCD contributions and higher twists (e.g., the Cahn effect in SIDIS).

B. The SSA in SIDIS

In the following, all displayed experimental data for weighted SSA in SIDIS were collected by the HERMES collaboration at the cm energy squared $s = 56.2$ GeV^2 and the average scale $\langle Q^2 \rangle = 2.5$ GeV^2 (but evolution effects were included for each $Q^2(x)$ in the x distribution). Applied experimental cuts are:

$$0.023 < x < 0.4\,, \qquad 0.2 < z < 0.8\,,$$
$$y_{\min}(x) < y < 0.85\,, \qquad y_{\min}(x) = \max\left[0.1,\, \frac{1}{x(s-M^2)},\, \frac{4-M^2}{(1-x)\,(s-M^2)}\right]\,. \tag{96}$$

Particular care must be taken when considering the asymmetry as a function of z, namely when separately integrating its numerator and denominator as functions of x and y.

In Fig. 7, we show the x dependence of the virtual photon asymmetry A_1 from Eq. (10). Experimental data for both π^+ (left) and π^- emission (right) are taken from Ref. [22] in the above mentioned SIDIS kinematics of HERMES.

In all cases, the solid line is the result of our spectator model when employing the fragmentation function D_1 of Ref. [55], including LO evolution of all partonic densities to the experimental scale. The agreement with data is

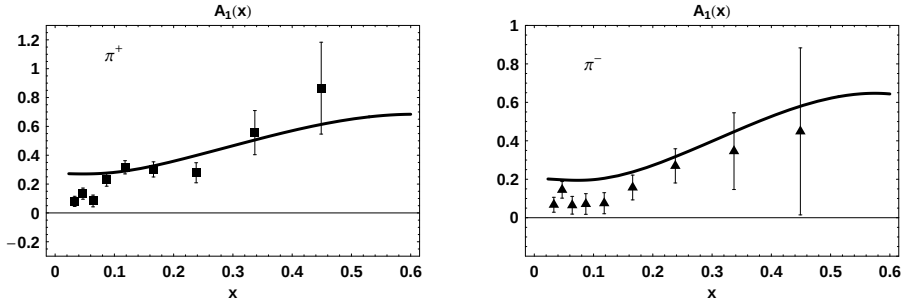

FIG. 7: The double-spin asymmetries $A_1(x)$ from Eq. (10) (see text) in the SIDIS kinematics of HERMES with emission of π^+ (left) and π^- (right). Experimental data from Ref. [22]. Solid line represents the result of the spectator model.

satisfactory. The deviations from data at low x are driven by contributions of nonvalence partons (sea quarks), which are not included in the present version of the model (see the comment at the beginning of Sec. IV).

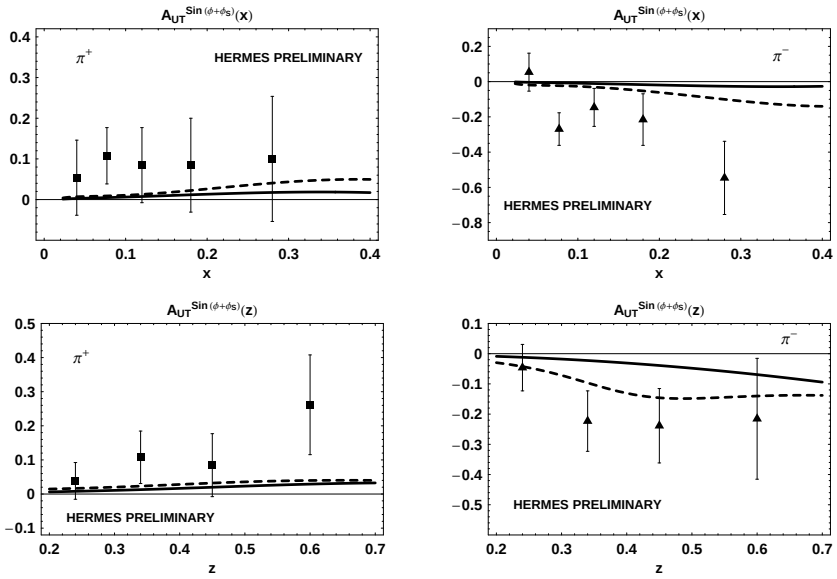

FIG. 8: The weighted single-spin asymmetry $A_{UT}^{Q_T\ \sin(\phi_h+\phi_S)}$ of Eq. (12) in the SIDIS kinematics of HERMES (Collins effect) with emission of π^+ (left) and π^- (right), as a function of x (above) and z (below). Experimental data from Ref. [15]. Dashed line for the result of the spectator model at its scale $Q_0^2 = 0.3$ GeV^2, solid line for the result at the experimental scale $Q^2 = 2.5$ GeV^2 (see text for details about evolution).

In Fig. 8, we show the x (top panels) and z (bottom panels) dependences of the weighted SSA $A_{UT}^{Q_T\ \sin(\phi_h+\phi_S)}$ from Eq. (12) for both π^+ (left) and π^- emission (right) in the same SIDIS kinematics of HERMES as in the previous figure (Collins effect [73]). Experimental data are taken from Ref. [15]. The dashed line represents the result of the SSA when calculating it at the model scale $Q_0^2 = 0.3$ GeV^2, where the analytic expression of the Collins function $H_1^\perp$ is taken from the consistent spectator approach of Ref. [56]; the D_1 of Ref. [55] has been down-evolved at LO using again the HOPPET code [57]. The solid line is the result for the SSA evolved at LO to the experimental scale $Q^2 = 2.5$ GeV^2.

The agreement with data is satisfactory but for the unfavoured channel of π^- emission, probably because of the approximation introduced into the description of the Collins function for this case [56]. The effect of DGLAP evolution is not large, suggesting that there are compensations between the numerator and denominator of the SSA.

In Fig. 9, we show the x (above) and z (below) dependences of the weighted SSA $A_{UT}^{Q_T\ \sin(\phi_h-\phi_S)}$ from Eq. (13) for both π^+ (left) and π^- emission (right) in the same SIDIS kinematics of HERMES as in the previous figures (Sivers effect [52]). Experimental data are taken from Ref. [15]. The dashed line represents the result of the weighted SSA when calculating it at the model scale $Q_0^2 = 0.3$ GeV^2 by down-evolving the D_1 of Ref. [55] at LO using again the

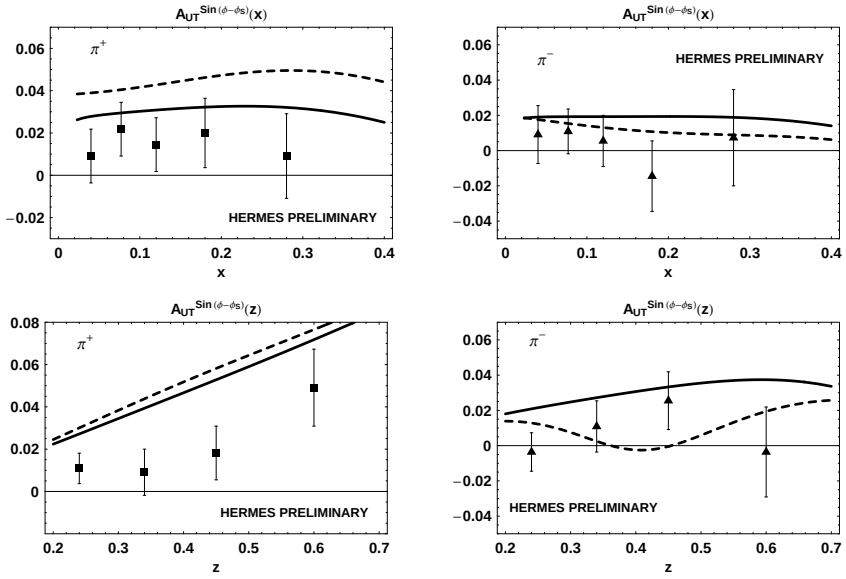

FIG. 9: The weighted single-spin asymmetry $A_{UT}^{Q_T\ \sin(\phi_h-\phi_S)}$ of Eq. (13) in the SIDIS kinematics of HERMES (Sivers effect [52]) with emission of π^+ (left) and π^- (right), as a function of x (above) and z (below). Experimental data from Ref. [15]. Dashed and solid lines with the same notations as in previous figure.

HOPPET code [57]. The solid line is the result for the weighted SSA evolved at LO to the experimental scale $Q^2 = 2.5$ GeV^2.

The agreement between our results and the data is good for the x dependence, while a discrepancy is evident for the z distribution in the π^+ channel. As already anticipated at the beginning of Sec. IV, the lacking of a strong sea–quark contribution at small x (in our model, it is generated only by radiative corrections) may deplete the denominator of the SSA once integrated upon x, and produce the observed enhancement upon data in the z distribution (in the numerator, the Sivers function is less affected by sea quarks).

In Fig. 10, we show our predictions for the x dependence of the weighted SSA $A_{UT}^{Q_T\ \sin(\phi_h+\phi_S)}$ of Eq. (12) (Collins effect), $A_{UT}^{Q_T\ \sin(\phi_h-\phi_S)}$ of Eq. (13) (Sivers effect), and $A_{LT}^{Q_T\ \cos(\phi_h-\phi_S)}$ of Eq. (14), for the reaction $n^\uparrow(e, e'\pi^\pm)$. The measurement was recently performed at Hall A of JLab by the E06-010 and E06-011 collaborations [24], using a 6 GeV energy beam and a transversely polarized ^{3}He (effective neutron) target in SIDIS kinematics with cm energy squared $s = 12.14$ GeV^2, average scale $\langle Q^2\rangle = 2.2$ GeV^2 and the following experimental cuts:

$$0.13 < x < 0.4\,, \qquad 0.46 < z < 0.59\,,$$
$$y_{\min}(x) < y < 0.86\,, \qquad y_{\min}(x) = \max\left[0.68,\ \frac{1.3}{x(s-M^2)},\ \frac{5.4-M^2}{(1-x)\,(s-M^2)}\right]\,. \tag{97}$$

In each panel of Fig. 10, the solid (dashed) line represents the result for the emission of π^+ (π^-) in the above kinematics. All components of the weighted SSA have been evolved at LO to the experimental average scale $Q^2 = 2.2$ GeV^2 using the HOPPET code [57]. The LO evolution kernels for the transversity and the first $\boldsymbol{p}_T$ moment of the Sivers function are the same as those ones used in Fig. 8 and 9, respectively. The evolution of $g_{1T}^{(1)}$ is assumed at LO to be the same as the one of the helicity distribution g_1.

C. The SSA in Drell–Yan

As there are no data for weighted SSA in Drell–Yan collisions, we will show our predictions for cases of interest in view of future experiments. At FAIR (GSI), the PAX collaboration is planning to measure the fully polarized Drell–Yan process with antiprotons in order to perform a self-consistent extraction of the transversity distribution [25–29]. Moreover, by simply switching on and off the transverse polarization of only one hadron, from the combination of the various cross sections it is possible to extract h_1 also together with the Boer–Mulders function $h_1^\perp$ [see Eqs. (31, 32)]. Finally, using the same process the COMPASS collaboration is planning to extract the Sivers function using a high

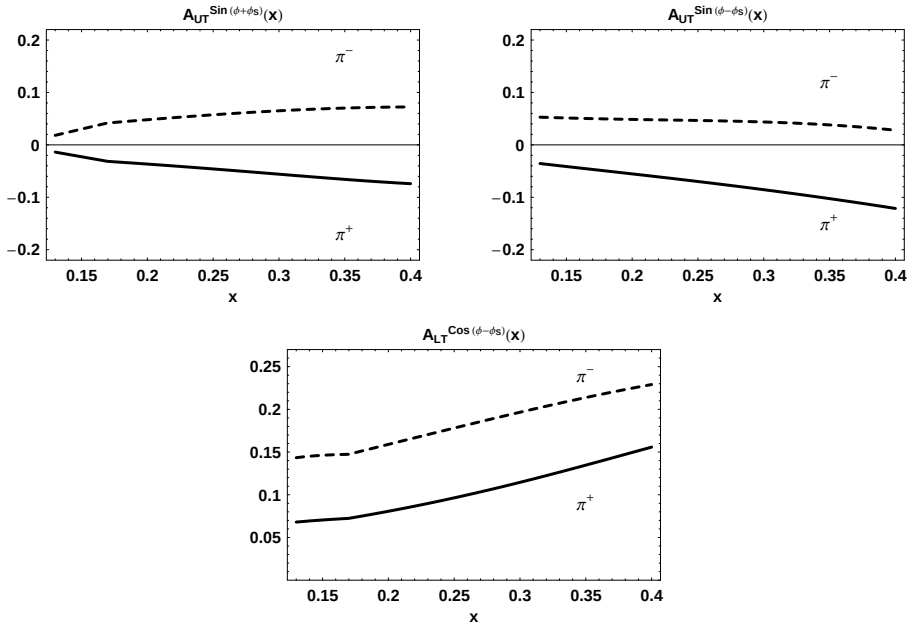

FIG. 10: The weighted single-spin asymmetries $A_{UT}^{Q_T\ \sin(\phi_h+\phi_S)}$ of Eq. (12) (Collins effect), $A_{UT}^{Q_T\ \sin(\phi_h-\phi_S)}$ of Eq. (13) (Sivers effect), $A_{LT}^{Q_T\ \cos(\phi_h-\phi_S)}$ of Eq. (14), as functions of x in the SIDIS kinematics at JLab with a 6 GeV beam energy for the emission of π^+ (solid line) and π^- (dashed line) from a transversely polarized neutron [24].

energetic pion beam on a transversely polarized proton target at CERN [30–33], in order to directly test its predicted non-universal behaviour [34].

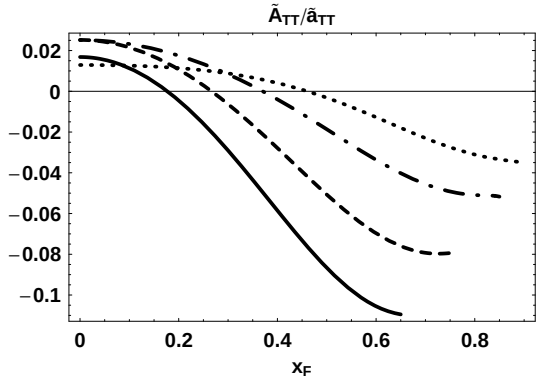

FIG. 11: The double-spin asymmetry $\tilde{A}_{TT}/\tilde{a}_{TT}$ of Eq. (25) as a function of x_F for the $\bar{p}^\uparrow p^\uparrow \to \mu^+\mu^- X$ process at the PAX kinematics (see text). Solid, dashed, dot-dashed, and dotted lines correspond to c.m. energies squared s = 30, 45, 80, 200 GeV^2, respectively.

In Fig. 11, we show our prediction for the x_F dependence of the double-spin asymmetry $\tilde{A}_{TT}/\tilde{a}_{TT}$ from Eq. (25) for the $\bar{p}^\uparrow p^\uparrow \to \mu^+\mu^- X$ process that could be studied at PAX with a fully transversely polarized antiproton beam ($|\boldsymbol{S}_{1T}| = 1$) colliding on a fully ($|\boldsymbol{S}_{2T}| = 1$) transversely polarized proton target [25, 27]. Conventions are according to Eq. (22). Dimuon invariant masses are summed in the range $2 < M < 3$ GeV, below the J/ψ resonance. Solid, dashed, dot-dashed, and dotted lines correspond to c.m. energies squared $s = 30$, 45, 80, 200 GeV^2, respectively. All the parton distributions entering the asymmetry are evolved at LO to each $Q^2 \equiv M^2$ inside the integration range.

Despite the fact that $\tilde{A}_{TT}$ is roughly the "squared" of the transversity distribution, it does change sign for some x_F depending on the value of s. As it is evident from Eq. (22), for different s the same x_F and M probe different x_1 and x_2, and, in particular, those where one of the two model transversities for quark up changes sign (see Fig. 8 of Ref. [10]). Consequently, the asymmetry of Eq. (25) also changes sign. This feature contrasts with other results

in the literature [27, 28, 74, 75]. Moreover, we also see a monotonically decreasing trend in x_F (and also in y), but our asymmetry is as large as 10% in modulus at most. This is probably due to cancellations that occur when summing upon the invariant mass M, or equivalently when integrating upon specific portions of the (x_1, x_2) phase space, where the product $h_1^{\overline{u}}(x_1)\, h_1^u(x_2)$ in $\tilde{A}_{TT}$ repeatedly changes sign [and is comparable with, or bigger than, the positive $h_1^{\overline{d}}(x_1)\, h_1^d(x_2)$]. For both reasons, a measure of $\tilde{A}_{TT}$ is highly desirable because it would also clarify the issue.

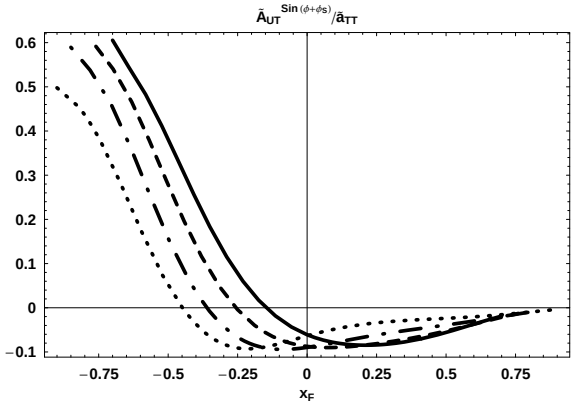

FIG. 12: The weighted single-spin asymmetry $\tilde{A}_{UT}^{q_T\,\sin(\phi+\phi_{S_2})}/\tilde{a}_{TT}$ of Eq. (32) for the $\bar{p}p^\uparrow \to \mu^+\mu^- X$ process as a function of x_F, in the same kinematics, conventions and notations, as in the previous figure.

In Fig. 12, we show our prediction for the x_F dependence of the weighted SSA $\tilde{A}_{UT}^{q_T\,\sin(\phi+\phi_{S_2})}/\tilde{a}_{TT}$ from Eq. (32) for the $\bar{p}p^\uparrow \to \mu^+\mu^- X$ process that could be studied at PAX with antiproton beams colliding on a transversely polarized proton target [25, 46, 47]. Conventions and notations are the same as in the previous figure. Evolution effects are included for all partonic densities; as already explained at the end of Sec. II B, the LO evolution equations of the chiral-odd $h_1^{\perp(1)}$ are assumed to be the same as those of the chiral-odd transversity h_1. The outcome in Fig. 12 already takes into account the predicted sign change of T-odd TMDs when going from SIDIS to Drell–Yan collisions [34].

Again, for different s the same x_F and M probe different x_1 and x_2, in particular the range where the $h_1^u(x_2)$ changes sign. Consequently, the asymmetry of Eq. (32) also changes sign, the turning point depending on s. For the very same reason, cancellations probably occur when summing upon the invariant mass M, which suppress the size of the asymmetry at positive x_F. On the contrary, the size of $\tilde{A}_{UT}^{q_T\,\sin(\phi+\phi_{S_2})}/\tilde{a}_{TT}$ is significant at negative x_F. .

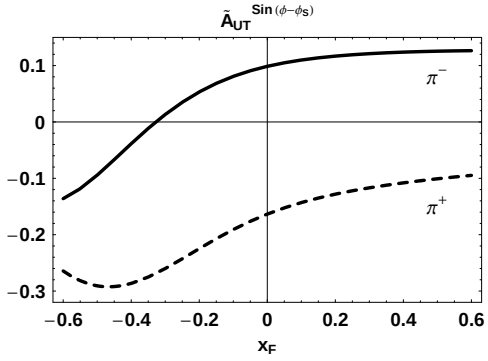

FIG. 13: The weighted single-spin asymmetry $\tilde{A}_{UT}^{q_T\,\sin(\phi-\phi_{S_2})}$ of Eq. (31) as a function of x_F for the $\pi p^\uparrow \to \mu^+\mu^- X$ process at COMPASS (see text). Upper solid (lower dashed) line for π^- (π^+).

In Fig. 13, we show our prediction for the x_F dependence of the weighted SSA $\tilde{A}_{UT}^{q_T\,\sin(\phi-\phi_{S_2})}$ from Eq. (31) for the $\pi p^\uparrow \to \mu^+\mu^- X$ process that could be studied at COMPASS with a 160 GeV pion beam colliding on a transversely polarized proton target [30, 31, 33]. Dimuon invariant masses are summed in the safe range $4 < M < 9$ GeV between the J/ψ and the Υ resonances; since $s = 300$ GeV^2, the invariant $\tau \approx 0.16$ is in the valence region. Other kinematic

onventions are the same as in the previous figure. Again, the result already takes into account the predicted sign change of T-odd TMDs when going from SIDIS to Drell–Yan collisions [34].

Following Ref. [30], we approximate the $\tilde{A}_{UT}^{q_T \sin(\phi-\phi_{S_2})}$ of Eq. (31) by considering only the dominant valence contribution to the $\pi - p$ collision. Therefore, for π^- (π^+) we retain only the $\bar{u} - u$ ($\bar{d} - d$) annihilation and the final weighted SSA does no longer depend on the partonic densities in the pion. Evolution effects are included at LO along the lines described at the end of Sec. II A. The upper solid (lower dashed) line is our result for π^- (π^+).

The size of the asymmetry should allow for an unambiguous test of the prediction about the above mentioned sign change of the Sivers function with respect to its extraction from SIDIS [31].

V. CONCLUSIONS

In this paper, we have analytically calculated azimuthal (spin) asymmetries in lepton-nucleon semi-inclusive deep-inelastic scattering (SIDIS) and in Drell-Yan hadronic collisions, using the leading-twist transverse-momentum dependent distributions (TMDs) obtained in the diquark spectator model of the nucleon from Ref. [10].

We have included evolution effects at leading order (LO) in α_s by implementing in the HOPPET code of Ref. [57] the kernel for chiral-odd objects. While DGLAP equations are well known for the momentum $f_1(x)$, helicity $g_1(x)$, and transversity $h_1(x)$ distributions, we have included evolution effects in an approximate way also for the first $\boldsymbol{p}_T$ moments of the Sivers $f_{1T}^{\perp\,(1)}(x)$, $g_{1T}^{(1)}(x)$, and Boer-Mulders $h_1^{\perp\,(1)}(x)$ functions, as described in Sec. IV. Moreover, since in our model the first $\boldsymbol{p}_T$ moment of naïve T-odd densities depends linearly upon α_s at the model scale, a consistent treatment of evolution effects requires to determine α_s itself from the renormalization group equations. Therefore, with respect to Ref. [10] we have modified its value at the hadronic model scale Q_0^2: instead of using an *ad-hoc* nonperturbative input as a free parameter, we have computed $\alpha_s(Q_0^2)$ from the LO renormalization group equations. The net effect is a resizing of all T-odd functions by a global constant. The comparison with available parametrizations [59, 65, 66] is encouraging for the Sivers function, but requires more investigations in the case of the Boer-Mulders one.

We have tested our model TMDs by considering weighted single-spin asymmetries (SSA) in both SIDIS and Drell–Yan collisions. Data for weighted SSA are scarce, with low statistics, and still preliminary [15, 22]. But, from the theoretical side they are preferable than unweighted SSA because in a model independent way their final expressions get automatically factorized involving simple products of "collinear" objects [16] – parton distribution functions (PDFs) or $\boldsymbol{p}_T$ moments of TMDs (and analogously for fragmentation functions). As such, weighted SSA can be always calculated analytically in our model. Incidentally, the choice of considering evolution effects only at LO is dictated by the consistency with the expressions for the weighted SSA, which are known at LO.

As for SIDIS, we have considered the asymmetry A_{LL} with longitudinally polarized protons [22], and the Collins and the Sivers effects [15], all measured by the HERMES collaboration; we have made predictions for the Collins and the Sivers effects, as well as for A_{LT}, in the kinematic conditions recently explored in the E06-010 and E06-011 experiments in Hall A at JLab [24], using the 6 GeV energy beam and the transversely polarized ^{3}He effective neutron target. For the unpolarized fragmentation function D_1, we have adopted the parametrization of Ref. [55], while we have used the analytic expression of the Collins function from Ref. [56], obtained using a spectator approach similar to the present framework. Overall, the comparison with experimental data is satisfactory. For the Collins effect, in some cases there are discrepancies that probably can be traced back to the assumptions made in the description of the unfavoured channels of the Collins function [56].

Since there are no data for weighted SSA in Drell–Yan collisions, we have made predictions for cases of interest in view of future experiments. At FAIR (GSI), the PAX collaboration is planning to measure the fully polarized Drell–Yan process with antiprotons in order to perform a self-consistent extraction of the transversity distribution [25–29]; we have presented our predictions for $\tilde{A}_{TT}$ in various kinematic configurations. Interestingly, despite the fact that this asymmetry is approximately the "squared" of the transversity distribution h_1, our $\tilde{A}_{TT}$ does change sign in some portions of the phase space. Briefly, the kinematics of the parton-antiparton annihilation explores different ranges in the x dependence of the two involved h_1, which can separately become negative in our model (see Fig. 8 of Ref. [10]). This feature contrasts with other results in the literature [27, 28, 74, 75]; it would be highly desirable to measure $\tilde{A}_{TT}$ in order to clarify this issue.

By simultaneously considering Drell–Yan collisions where both hadrons are unpolarized or only one is transversely polarized, it is possible to measure a weighted SSA that leads to the extraction of h_1 in combination with the Boer-Mulders function $h_1^\perp$. We have presented our predictions again in the kinematic regime that the PAX collaboration could explore at FAIR (GSI). The same previous comment on the sign of h_1 applies here too.

Finally, using the same process (single-polarized Drell–Yan collision) the COMPASS collaboration is planning to extract the Sivers function using a high energetic pion beam on a transversely polarized proton target at CERN [30–

33], in order to directly test its predicted non-universal behaviour [34]. We have shown our predictions for both π^- and π^+ collisions, assuming that the elementary annihilation is driven by the dominant valence contributions.

Acknowledgments

This work was partially supported by the Research Infrastructure Integrated Activity "Study of Strongly Interacting Matter" (acronym HadronPhysics2, grant agreement n. 227431) under the 7^{th} Framework Programme of the European Community, and by the Italian MIUR through the PRIN 2008EKLACK "Structure of the nucleon: transverse momentum, transverse spin and orbital angular momentum".

[1] J. C. Collins and D. E. Soper, Nucl. Phys. **B194**, 445 (1982).
[2] S. J. Brodsky, D. S. Hwang, and I. Schmidt, Phys. Lett. **B530**, 99 (2002), hep-ph/0201296.
[3] S. J. Brodsky, D. S. Hwang, and I. Schmidt, Nucl. Phys. **B642**, 344 (2002), hep-ph/0206259.
[4] M. Burkardt and D. S. Hwang, Phys. Rev. **D69**, 074032 (2004), hep-ph/0309072.
[5] K. Goeke, S. Meissner, A. Metz, and M. Schlegel, Phys. Lett. **B637**, 241 (2006), hep-ph/0601133.
[6] Z. Lu and I. Schmidt, Phys. Rev. **D75**, 073008 (2007), hep-ph/0611158.
[7] S. Meissner, A. Metz, and K. Goeke, Phys. Rev. **D76**, 034002 (2007), hep-ph/0703176.
[8] J.-W. Qiu, W. Vogelsang, and F. Yuan, Phys. Rev. **D76**, 074029 (2007), arXiv:0706.1196 [hep-ph].
[9] M. Burkardt and B. Hannafious, Phys. Lett. **B658**, 130 (2008), arXiv:0705.1573 [hep-ph].
[10] A. Bacchetta, F. Conti, and M. Radici, Phys. Rev. **D78**, 074010 (2008), 0807.0323.
[11] S. Chekanov et al. (ZEUS), Phys. Rev. **D67**, 012007 (2003), hep-ex/0208023.
[12] M. Glück, E. Reya, M. Stratmann, and W. Vogelsang, Phys. Rev. **D63**, 094005 (2001), hep-ph/0011215.
[13] A. Airapetian et al. (HERMES), Phys. Rev. Lett. **94**, 012002 (2005), hep-ex/0408013.
[14] A. Bressan (COMPASS) (2009), 0907.5508.
[15] R. Seidl (HERMES) (2004), prepared for 12th International Workshop on Deep Inelastic Scattering (DIS 2004), Strbske Pleso, Slovakia, 14-18 Apr 2004.
[16] P. J. Mulders and R. D. Tangerman, Nucl. Phys. **B461**, 197 (1996), erratum-ibid. **B484** (1997) 538, hep-ph/9510301.
[17] M. Guagnelli, A. Bacchetta, and M. Radici (in preparation).
[18] S. Boffi, A. V. Efremov, B. Pasquini, and P. Schweitzer, Phys. Rev. **D79**, 094012 (2009), 0903.1271.
[19] Z.-B. Kang and J.-W. Qiu, Phys. Rev. **D79**, 016003 (2009), 0811.3101.
[20] W. Vogelsang and F. Yuan, Phys. Rev. **D79**, 094010 (2009), 0904.0410.
[21] V. M. Braun, A. N. Manashov, and B. Pirnay, Phys. Rev. **D80**, 114002 (2009), 0909.3410.
[22] A. Airapetian et al. (HERMES), Phys. Rev. **D71**, 012003 (2005), hep-ex/0407032.
[23] M. Alekseev et al. (COMPASS), Phys. Lett. **B680**, 217 (2009), 0905.2828.
[24] JLab experiment E06-010/E06-011, J.-P. Chen, E. Cisbani, H. Gao, X. Jiang, J.-C. Peng, spokespersons.
[25] V. Barone et al. (PAX) (2005), hep-ex/0505054.
[26] M. Maggiora et al. (ASSIA), Czech. J. Phys. **55**, A75 (2005), proceedings of the ASI Conference on Symmetries and Spin (Spin-Praha 2004), Praha, 5-10 July 2004., hep-ex/0504011.
[27] A. V. Efremov, K. Goeke, and P. Schweitzer, Eur. Phys. J. **C35**, 207 (2004), hep-ph/0403124.
[28] M. Anselmino, V. Barone, A. Drago, and N. N. Nikolaev, Phys. Lett. **B594**, 97 (2004), hep-ph/0403114.
[29] A. Bianconi and M. Radici, Phys. Rev. **D72**, 074013 (2005), hep-ph/0504261.
[30] A. V. Efremov, K. Goeke, S. Menzel, A. Metz, and P. Schweitzer, Phys. Lett. **B612**, 233 (2005), hep-ph/0412353.
[31] A. Bianconi and M. Radici, Phys. Rev. **D73**, 114002 (2006), hep-ph/0602103.
[32] A. Bianconi and M. Radici, Phys. Rev. **D73**, 034018 (2006), hep-ph/0512091.
[33] M. Anselmino et al., Phys. Rev. **D79**, 054010 (2009), 0901.3078.
[34] J. C. Collins, Phys. Lett. **B536**, 43 (2002), hep-ph/0204004.
[35] A. Bacchetta, M. Diehl, K. Goeke, A. Metz, P. J. Mulders, and M. Schlegel, JHEP **02**, 093 (2007), hep-ph/0611265.
[36] A. Bacchetta, D. Boer, M. Diehl, and P. J. Mulders, JHEP **08**, 023 (2008), 0803.0227.
[37] D. Boer and P. J. Mulders, Phys. Rev. **D57**, 5780 (1998), hep-ph/9711485.
[38] J. Zhou, F. Yuan, and Z.-T. Liang (2009), 0909.2238.
[39] V. Barone, A. Drago, and P. G. Ratcliffe, Phys. Rept. **359**, 1 (2002), hep-ph/0104283.
[40] M. Stratmann and W. Vogelsang, Phys. Rev. **D65**, 057502 (2002), hep-ph/0108241.
[41] J. C. Collins, D. E. Soper, and G. Sterman, Nucl. Phys. **B250**, 199 (1985).
[42] J. C. Collins and D. E. Soper, Phys. Rev. **D16**, 2219 (1977).
[43] S. Arnold, A. Metz, and M. Schlegel (2008), 0809.2262.
[44] R. D. Tangerman and P. J. Mulders, Phys. Rev. **D51**, 3357 (1995), hep-ph/9403227.
[45] D. Boer, Phys. Rev. **D60**, 014012 (1999), hep-ph/9902255.
[46] A. Bianconi and M. Radici, Phys. Rev. **D71**, 074014 (2005), hep-ph/0412368.

[47] M. Radici, F. Conti, A. Bacchetta, and A. Bianconi (2007), arXiv:0708.0232 [hep-ph], URL http://www.slac.stanford.edu/spires/find/hep/www?eprint=arXiv:0708.0232.
[48] R. Jakob, P. J. Mulders, and J. Rodrigues, Nucl. Phys. **A626**, 937 (1997), hep-ph/9704335.
[49] H. Avakian, A. V. Efremov, P. Schweitzer, and F. Yuan, Phys. Rev. **D78**, 114024 (2008), 0805.3355.
[50] A. V. Efremov, P. Schweitzer, O. V. Teryaev, and P. Zavada (2008), 0812.3246.
[51] J. She, J. Zhu, and B.-Q. Ma, Phys. Rev. **D79**, 054008 (2009), 0902.3718.
[52] D. W. Sivers, Phys. Rev. **D41**, 83 (1990).
[53] D. Boer, P. J. Mulders, and F. Pijlman, Nucl. Phys. **B667**, 201 (2003), hep-ph/0303034.
[54] A. Bacchetta, M. Boglione, A. Henneman, and P. J. Mulders, Phys. Rev. Lett. **85**, 712 (2000), hep-ph/9912490.
[55] D. de Florian, R. Sassot, and M. Stratmann, Phys. Rev. **D75**, 114010 (2007), hep-ph/0703242.
[56] A. Bacchetta, L. P. Gamberg, G. R. Goldstein, and A. Mukherjee, Phys. Lett. **B659**, 234 (2008), 0707.3372.
[57] G. P. Salam and J. Rojo, Comput. Phys. Commun. **180**, 120 (2009), 0804.3755.
[58] M. Glück, E. Reya, and A. Vogt, Eur. Phys. J. **C5**, 461 (1998), hep-ph/9806404.
[59] M. Anselmino et al., Eur. Phys. J. **A39**, 89 (2009), 0805.2677.
[60] J. C. Collins et al. (2005), hep-ph/0510342.
[61] M. Diefenthaler (HERMES) (2007), proceedings of the 15th International Workshop on Deep Inelastic Scattering (DIS 2007), Munich, Germany, 16 - 20 Apr 2007., 0706.2242.
[62] A. Martin (COMPASS), Czech. J. Phys. **56**, F33 (2006), hep-ex/0702002.
[63] M. Alekseev et al. (COMPASS), Phys. Lett. **B673**, 127 (2009), 0802.2160.
[64] M. Gockeler et al. (QCDSF), Phys. Rev. Lett. **98**, 222001 (2007), hep-lat/0612032.
[65] V. Barone, S. Melis, and A. Prokudin (2009), 0912.5194.
[66] Z. Lu and I. Schmidt (2009), 0912.2031.
[67] W. Kafer (COMPASS) (2008), 0808.0114.
[68] A. Bressan (COMPASS) (2009), 0907.5511.
[69] F. Giordano and R. Lamb (On behalf of the HERMES), AIP Conf. Proc. **1149**, 423 (2009), 0901.2438.
[70] L. Y. Zhu et al. (FNAL E866/NuSea), Phys. Rev. Lett. **102**, 182001 (2009), 0811.4589.
[71] L. P. Gamberg, G. R. Goldstein, and M. Schlegel, Phys. Rev. **D77**, 094016 (2008), 0708.0324.
[72] F. Yuan, Phys. Lett. **B575**, 45 (2003), hep-ph/0308157.
[73] J. C. Collins, Nucl. Phys. **B396**, 161 (1993), hep-ph/9208213.
[74] V. Barone, A. Cafarella, C. Coriano', M. Guzzi, and P. Ratcliffe, Phys. Lett. **B639**, 483 (2006), hep-ph/0512121.
[75] B. Pasquini, M. Pincetti, and S. Boffi, Phys. Rev. **D76**, 034020 (2007), hep-ph/0612094.